We are IntechOpen,
the world's leading publisher of
Open Access books
Built by scientists, for scientists

4,800
Open access books available

122,000
International authors and editors

135M
Downloads

Our authors are among the

154
Countries delivered to

TOP 1%
most cited scientists

12.2%
Contributors from top 500 universities

CLARIVATE ANALYTICS
BOOK CITATION INDEX
INDEXED

WEB OF SCIENCE™

Selection of our books indexed in the Book Citation Index
in Web of Science™ Core Collection (BKCI)

Interested in publishing with us?
Contact book.department@intechopen.com

Numbers displayed above are based on latest data collected.
For more information visit www.intechopen.com

Stimulated Raman Scattering with a Relativistic Vlasov-Maxwell Code: Cascades of Nonstationary Nonlinear Kinetic Interactions

Magdi Shoucri and Bedros Afeyan

Additional information is available at the end of the chapter

1. Introduction

In laser fusion, hundreds of laser beams propagate through underdense coronal (ablator material) plasmas surrounding the Deuterium-Tritium (fusion fuel) filled target. At least tens of targets would have to be irradiated in succession per second for laser fusion energy cycle economics to be viable with modest or high (50-100) gain targets. The propagation of multiple laser beams in this coronal plasma and the subsequent energy deposition must be well controlled to achieve thermonuclear ignition and significant gain [1]. Because of high laser intensities and long plasma scalelengths, the underdense plasma environment is invariably the scene of nonlinear coherent processes which are detrimental to laser fusion. This is because they can lead to backscattering losses, hot electron preheating and implosion non-uniformity. Considerable attention has been given to parametric instabilities or nonlinear optical processes in plasmas (for an entry level introduction, see [2]). The linear theory of such instabilities is well understood (see [3-6] for high frequency parametric instabilities involving electron plasma waves (EPW)) but the nonlinear kinetic theory is still rich with mysteries to be uncovered (for an introduction with some advanced elements see the recent text in [7]). This is because kinetic effects add new dimensions of velocity space dynamics, changing the distribution functions strongly (away from a dull Maxwellian) and making the resonant wave-wave interaction picture much more intricate via wave-particle and particle-particle interactions (see [8,9] for an older perspective, and [10] for a more in depth and modern one). In particular, trapping, untrapping and retrapping of (a sufficiently large number of) particles makes the *transient* behaviour well beyond the reach of nonlinear knob-kludged fluid models. Coherent, phase sensitive, nonlocal memory effects, disparate scales and bursty or intermittent structures, all make predictions difficult, toy models irrelevant, and useful simulations very

challenging. In particular, the initiation of large backscattering, for instance, may depend on many processes that precede that growth in leading the distribution function away from a Maxwellian, which, had it not changed, would not have allowed backscattering growth at all.

In the present work, we apply an Eulerian Vlasov code for the numerical simulation of the one-dimensional (1D) relativistic Vlasov-Maxwell equations, to study the laser-plasma interaction process known as stimulated Raman scattering (SRS). The Eulerian Vlasov code we use was presented and applied in several references [11-16]. The numerical scheme applies a direct solution method of the Vlasov equation as a partial differential equation in phase-space without dimensional splitting. The numerical scheme is based on a 2D advection technique, of second-order accuracy in time-step. The distribution function is advanced in time by interpolating in 2D along the phase space characteristic using a tensor product of cubic *B*-spline. Interest in Eulerian grid-based solvers associated with the method of characteristics for the numerical simulation of the Vlasov equation comes from the very low noise levels inherent in these codes, which allow us to study accurately nonlinear physics in low density regions of phase-space (see also [17]), without being inundated by numerical artifacts.

Besides SRBS, and SRFS, which is the analogous Raman forward scattering instability, other high frequency instabilities may occur at least kinetically when modified distribution functions exist (see [5,6,18-20]). In the family of such structures, which are beyond the scope of fluid models, are stimulated scattering off Electron Acoustic Waves (EAW) and Kinetic Electrostatic Electron Nonlinear (KEEN) waves. These stimulated processes are therefore called SEAS and SKEENS. There are also Beam Acoustic Modes (BAM) having been identified as possibly being linked to SRBS nonlinear evolution and saturation (see for instance [21-23]). A different perspective has also been promulgated under the heading of transient enhanced instability levels attributed to rapidly changing distribution functions which diminish damping rates and thus allow larger levels of SRS than would be expected in models ignoring transient tracking of distribution functions. These come under the heading of inflationary models of SRS.

Of these, KEEN waves have the interesting feature that they do not require a pre-flattened (zero slope at the phase velocity of the wave) distribution function and are not steady-state, time-independent solutions. In other words, they are not BGK modes (see for instance [8,9]). On the other hand, EAWs and nonlinear EPWs are BGK modes. In contrast, KEEN waves involve multiple phase-locked harmonics which produce a steepened multi-mode electric field pattern that can throw particles a good distance ahead as untrapped particles which then may become retrapped and help maintain an overall wave amplitude that is not in strict local equilibrium with the plasma particle distribution. The slope of the averaged distribution function need not be zero anywhere (a necessity for EPW and EAW and BGK modes, or for stationarity) and there is no infinitesimal amplitude version of KEEN waves which are nonlinearly strongly modified phase space distribution function states. They were discovered by Afeyan *et al.* in 2002 while performing ponderomotively driven Vlasov-Poisson simulations, and while trying to explore the limits of resonance physics of EAWs. The latter were found to be of measure zero compared to KEEN waves. This was first published in the proceedings of the 2003 IFSA meeting [18].

Returning to the choice of a Vlasov code over a PIC code, say, we offer this argument. If some violent rapidly and strongly driven regime is adopted in a PIC simulation, say, solely to render the initial conditions of an underesolved model less troubling, then all such intricate physics (as found here) might go unnoticed. Or if all diagnostics that can be afforded after massively parallel and data distributed simulations only look at time averaged or time integrated quantities, again, the transient and exciting initiation processes might go unnoticed or obscured by much larger final state signatures. This is what we avoid here, and it appears the sequence of events in time that are revealed here have not been seen before by PIC or Vlasov code studies.

What causes the pre-distortion of distribution functions can easily be missed or miscalculated if coarse means of tracking the fine scale structures of phase space are adopted. This is an inherent risk in PIC codes. Typical practitioners tend to emphasize very rapidly imposed and large amplitude perturbations since otherwise they would risk drowning in slowly brewing, artificial-noise generated physics. Even with Vlasov codes, the important transient kinetic physics can be easily missed if the backscattered process is strongly promoted over all other processes by seeding it externally and artificially. Not allowing the plasma to develop its own response as it sees fit, when confronted with a high intensity laser and in the presence of thermal level plasma fluctuations, leads to blocking many phase space pathways of self-organization beyond just the backscattering channel. Instead of just stimulated Raman backscattering (SRBS), in a plasma at a given density and temperature (for sufficiently large wave vector-Debye length product values for stimulated Raman backscattering electron plasma waves, SRBS EPWs), one may also expect Raman forward scatter (SRFS), especially when the wavenumber of a small perturbation imposed in the plasma as an initial condition in the transverse field, corresponds to SRFS. We may then expect to see Kinetic Electrostatic Electron Nonlinear (KEEN) waves [18-20] driven by the pump beating with the backscattering portion of the imposed standing wave initial condition perturbation at the SRFS wavenumber. We observe that only after stimulated KEEN wave scattering, SKEENS, has caused sufficient KEEN wave growth, and the background distribution function sufficiently flattened, that Raman backscatter finally can develop in earnest. This is a novel scenario of SRBS initiation and entrenched entanglement with KEEN waves which coevolve even though eventually SRBS having the far superior growth rate outstrips the KEEN wave influence reaching even more nonlinear states later in time with positive slopes in the electron distribution function and the accompanying chaotic, bursty behaviour.

In this chapter we report new results that show that SRFS is first driven in such plasmas before SRBS can grow from small perturbations that do not directly seed it. We will show that SRFS will give rise to the excitation of KEEN waves due to the opposite direction wavenumber of the SRFS wave that was seeded by the initial scattered standing wave light field. This is then amplified by the pump through the SKEENS process. This then drives KEEN waves into their characteristic multiple-harmonic phase-locked structure and steepened electric field profiles which facilitate retrapping of particles that escape any given potential well as the overall electrostatic field adjusts to all these waves being driven and amplified. The back of the simulation box is where these processes coexist most markedly. In the middle of the simulation

box, SRBS finally grows after KEEN waves reach that area and change the local distribution function by softening it. SRBS eventually swallows up the KEEN wave and dominates since its growth rate is far higher. This new scenario confirms that nonlinear trapping evolution of SRBS is not just a question of EPWs but also of KEEN waves and SKEENS and that SRFS wavenumber perturbations can initiate the latter if a standing wave already exists much before SRBS can occur. The later evolution of all these processes is very complicated still involving positive slope electron distribution functions which will then accelerate the self-destruction of these modes and render the picture even more transient, intermittent and chaotic. We stop the simulations short of that eventuality where even Brillouin scatter begins to occur and dynamics and predictions become more challenging to track requiring ion acoustic waves and fluid saturation of SRS as well via Langmuir decay instability, etc.

Nonlocal and collective kinetic effects are involved in this physics. A direct Vlasov solver, capable of resolving these kinetic processes, is used here to address some aspects of the scattering properties of SRS and SKEENS. The code evolves relativistically both electrons and ions. In Vlasov codes used to simulate these problems, noise and other numerical fluctuations are very low for the SRBS to grow from, therefore it is usual in several simulations to stimulate artificially the counter-propagating daughter light wave at a low level as an injected seed, in order to enhance the SRBS growth and to allow the saturation phase to be reached rapidly. This saturation results from the competition of non-linear effects which include frequency shift, pump depletion, damping reduction, trapped particle instability, spatiotemporal chaos, among others. A detailed study of the resulting distribution function obtained at saturation has been presented, for instance, in Strozzi *et al*, 2007, which showed that the stage following saturation involved the transformation of Raman Langmuir waves into a set of beam acoustic modes or BAM (see also [24,25]), and an EAW appears at this stage with a weak reflected light that phase-matches for scattering off this mode, a process called electron acoustic scatter (EAS). SEAS has been experimentally observed in [26,27], and has been reported in simulations of plasmas overdense to SRBS and at relativistic pump intensities [11,28], and has been also observed in underdense Vlasov simulations [29]. Distinguishing between BAMs and EAWs is discussed in the literature, see for instance [22,29]. We will avoid this discussion, because they play secondary roles in the results presented here. For the parameters we are using, which involves strongly damped electron plasma waves, our simulations are dominated by SRFS, SKEENS and SRBS, in that order. It is the purpose of the present work to study these three processes and their mutual interactions, SRFS, SKEENS and SRBS which arise during the SRS dynamics process, and which appear in the early stage which precedes the saturation of the SRBS. To avoid any interference from artificially distorted distribution functions or imposed seeding, we start the code from an initial Maxwellian distribution, and the system evolves under the influence of a pump light wave which provides fluctuations from which SRS develops, without any additional imposed initial perturbation except for a standing wave at the resonant wavenumber of SRFS. This then develops SRFS but also drives SKEENS at the backscattering portion beating with the pump electrostatic ponderomotive field which seeds a KEEN wave directly. We do not seed the counter-propagating daughter light wave to stimulate the growth of the SRBS. We identify in the early phase of the Raman interaction a backscattered light that phase-matches for scattering off a KEEN wave, and which precedes

the growth and saturation of the SRBS process. These SKEENS events arise during the Raman physics, from the initial Maxwellian distribution. The signature of this KEEN wave is clearly identified in the electron distribution function phase-space, and the evolution of the system until the appearance of the growth and the saturation of the SRBS process will be followed. Possible effect of this SKEENS on the initiation and subsequent saturation of the SRBS process will be discussed.

2. The relevant equations of the Eulerian Vlasov code and the numerical scheme

We study this current problem by using an Eulerian Vlasov code for the numerical solution of the one-dimensional (1D) relativistic Vlasov-Maxwell equations. The relevant equations for the Eulerian Vlasov formulation are those previously presented in references [12-15] for instance. We present here these equations in order to fix the notation. Time t is normalized to the inverse plasma frequency ω_p^{-1}, length is normalized to $l_0 = c\omega_p^{-1}$, velocity and momentum are normalized respectively to the velocity of light c and to $M_e c$, where M_e is the electron mass and c is the velocity of light. We have the following Vlasov equations for the electrons and the ions distribution functions $f_{e,i}(x, p_{xe,i}, t)$:

$$\frac{\partial f_{e,i}}{\partial t} + \frac{p_{xe,i}}{\mu_{e,i}\gamma_{e,i}}\frac{\partial f_{e,i}}{\partial x} + \left(\mp E_x - \frac{1}{2\mu_{e,i}\gamma_{e,i}}\frac{\partial a_\perp^2}{\partial x}\right)\frac{\partial f_{e,i}}{\partial p_{xe,i}} = 0 \tag{1}$$

where $\gamma_{e,i} = \left(1 + (p_{xe,i}/\mu_{e,i})^2 + (a_\perp/\mu_{e,i})^2\right)^{1/2}$.

(the upper sign in Eq.(1) is for the electron equation and the lower sign for the ion equation, and subscripts e or i denote electrons or ions, respectively). In our normalized units $\mu_e = 1$ and $\mu_i = M_i/M_e$ is the ratio of ion to electron masses.

$$E_x = -\frac{\partial \phi}{\partial x} \text{ and } \vec{E}_\perp = -\frac{\partial \vec{a}_\perp}{\partial t} \tag{2}$$

and ϕ is given by Poisson's equation, which is given here by:

$$\frac{\partial^2 \phi}{\partial x^2} = \int f_e(x, p_{xe})dp_{xe} - \int f_i(x, p_{xi})dp_{xi} \tag{3}$$

The transverse electromagnetic fields E_y, B_z for the linearly polarized wave obey Maxwell's equations. Defining $E^\pm = E_y \pm B_z$, we have:

$$(\frac{\partial}{\partial t} \pm \frac{\partial}{\partial x})E^{\pm} = -J_y. \tag{4}$$

In our normalized units we have the following expressions for the normal current densities:

$$\vec{J}_{\perp} = \vec{J}_{\perp e} + \vec{J}_{\perp i} \; ; \quad \vec{J}_{\perp e,i} = -\frac{\vec{a}_{\perp}}{\mu_{e,i}} \int_{-\infty}^{+\infty} \frac{f_{e,i}}{\gamma_{e,i}} d p_{xe,i}.$$

The longitudinal electric field is calculated from Ampère's equation: $\partial E_x / \partial t = -J_x$ where

$$J_x = \frac{1}{\mu_i} \int_{-\infty}^{+\infty} \frac{p_{xi}}{\gamma_i} f_i \, dp_{xi} - \frac{1}{\mu_e} \int_{-\infty}^{+\infty} \frac{p_{xe}}{\gamma_e} f_e \, dp_{xe} \tag{5}$$

Test runs were made in which Poisson's equation was used instead of Ampère's equation to obtain the longitudinal electric field, with identical results.

The Eulerian Vlasov code we use to solve Eqs.(1-5) was recently presented and applied in [11-16] for instance. We outline the main steps for the numerical solution of Eq.(1), using an Eulerian scheme. Given $f_{e,i}^n$ at mesh points at time $t = n\Delta t$ (we stress here that the subscript i denotes the ion distribution function), we calculate the new value $f_{e,i}^{n+1}$ at the grid points j_x, and j_p corresponding to the mesh points $(x_{j_x}, p_{xe,i \, j_p})$ by writing that the distribution function is constant along the characteristics. The characteristics equations for Eq.(1) are given by:

$$\begin{aligned} \frac{dx}{dt} &= m_{e,i} \frac{p_{xe,i}}{\gamma_{e,i}} = V_{xe,i}(x, p_{xe,i}) \\ \frac{dp_{xe,i}}{dt} &= \mp E_x - \frac{m_{e,i}}{2\gamma_{e,i}} \frac{\partial a_{\perp}^2}{\partial x} = V_{p_{xe,i}}(x, p_{xe,i}). \end{aligned} \tag{6}$$

We assume that at the time $t_{n+1} \equiv t_n + \Delta t$, x is at the grid point j_x, and $p_{xe,i}$ is at the grid point j_p. The following leapfrog scheme can be written for the solution of (6):

$$\frac{x_{j_x} - x(t_n)}{\Delta t} = V_{xe,i}(x^{n+1/2}, p_{xe,i}^{n+1/2}) = V_{xe,i}(\frac{x_{j_x} + x(t_n)}{2}, \frac{p_{xe,i j_p} + p_{xe,i}(t_n)}{2}) \tag{7}$$

$$\frac{p_{xe,i j_p} - p_{xe,i}(t_n)}{\Delta t} = V_{p_{xe,i}}(x^{n+1/2}, p_{xe,i}^{n+1/2}) = V_{p_{xe,i}}(\frac{x_{j_x} + x(t_n)}{2}, \frac{p_{xe,i j_p} + p_{xe,i}(t_n)}{2}) \tag{8}$$

where $(x(t_n),\ p_{xe,i}(t_n))$ is the point where the characteristic is originating at t_n (not necessarily a grid point).

Put

$$\Delta_{xe,i} = \frac{x_{j_x} - x(t_n)}{2} \quad ;\ \Delta_{p_{xe,i}} = \frac{p_{xe,ij_p} - p_{xe,i}(t_n)}{2}. \tag{9}$$

Equations (7) and (8) can be rewritten as:

$$\Delta_{xe,i} = \frac{\Delta t}{2} V_{xe,i}(x_{j_x} - \Delta_{xe,i}, p_{xe,ij_p} - \Delta_{p_{xe,i}}). \tag{10}$$

$$\Delta_{p_{xe,i}} = \frac{\Delta t}{2} V_{p_{xe,i}}(x_{j_x} - \Delta_{xe,i}, p_{xe,ij_p} - \Delta_{p_{xe,i}}) \tag{11}$$

Which are implicit equations for $\Delta_{xe,i}$ and $\Delta_{p_{xe,i}}$ and are solved by iteration. This iteration is effected as follows. We rewrite Eqs.(10,11) in the vectorial form:

$$\Delta_{\mathbf{X}e,i} = \frac{\Delta t}{2} \mathbf{V}_{e,i}\left(\mathbf{X}_{e,i} - \Delta_{\mathbf{X}e,i}, t_{n+1/2}\right) \tag{12}$$

$X_{e,i}$ is the two dimensional vector $X_{e,i} = (x,\ p_{xe,i})$, and $\Delta_{X_{e,i}} = (\Delta_{xe,i},\ \Delta_{p_{xe,i}})$ is the two dimensional vector in Eq.(12) and $V_{e,i} = \left(V_{xe,i}^{n+1/2},\ V_{p_{xe,i}}^{n+1/2}\right)$. Eq.(12) for $\Delta_{X_{e,i}}$ is implicit and is solved iteratively by writing: $\Delta_{Xe,i}^{k+1} = \frac{\Delta t}{2} V_{e,i}(X_{e,i} - \Delta_{Xe,i}^{k}, t_{n+1/2})$, where we start the iteration with $\Delta_{Xe,i}^{0} = 0$ for $k=0$. Usually two or three iterations are sufficient to get a good convergence. The shifted values in Eqs.(10,11) are calculated by a two-dimensional interpolation using a tensor product of cubic *B*-splines [30]. We now write that the distribution function is constant along the characteristics. Then $f_{e,i}^{n+1}$ is calculated from $f_{e,i}^{n}$ from the relation :

$$f_{e,i}^{n+1}(x_{j_x}, p_{xe,ij_p}) = f_{e,i}^{n}(x(t_n), p_{xe,i}(t_n)) = f_{e,i}^{n}(x_{j_x} - 2\Delta_{xe,i}, p_{xe,i} - 2\Delta_{p_{xe,i}}). \tag{13}$$

Again the shifted values in Eq.(13) are calculated with a two-dimensional interpolation using a tensor product of cubic *B*-splines. Details have been presented in [30]. These methods

compared favourably with other Eulerian methods for the numerical solution of the Vlasov equation [31].

The numerical scheme to advance Eq.(1) from time t_n to t_{n+1} necessitates the knowledge of the electromagnetic field $E^{\pm}$ at time $t_{n+1/2}$. This is done using a centered scheme where we integrate Eq.(4) exactly along the vacuum characteristics with $\Delta x = \Delta t$, to calculate $E^{\pm n+1/2}$ as follows:

$$E^{\pm}(x \pm \Delta t, t_{n+1/2}) = E^{\pm}(x, t_{n-1/2}) - \Delta t J_y(x \pm \Delta t / 2, t_n) \qquad (14)$$

with $J_y(x \pm \Delta t / 2, t_n) = \dfrac{J_y(x \pm \Delta x, t_n) + J_y(x, t_n)}{2}$

From Eq.(2) we also have $\vec{a}_{\perp}^{n+1} = \vec{a}_{\perp}^{n} - \Delta t \vec{E}_{\perp}^{n+1/2}$, from which we calculate $\vec{a}_{\perp}^{n+1/2} = (\vec{a}_{\perp}^{n+1} + \vec{a}_{\perp}^{n}) / 2$. To calculate $E_x^{n+1/2}$, we use Ampère's equation: $\dfrac{\partial E_x}{\partial t} = -J_x$, from which $E_x^{n+1/2} = E_x^{n-1/2} - \Delta t J_x^{n}$.

3. The relevant parameters

We use a fine resolution grid in phase-space, with $N = 60000$ grid points in space, and 512 grid points in momentum space for the electrons and 256 grid points in momentum space for the ions (extrema of the electron momentum are ±0.5, and ±15 for the ion momentum). The initial distribution functions for the electrons and the ions are Maxwellian. The maximum of the density is normalized to $n = 0.0825 n_{cr}$, where n_{cr} is the critical density. The electron temperature is $T_e = 2$ keV. The ions have a temperature $T_i = 0.5$ keV. Ions are allowed to move, especially to adjust the sheath structure at the boundaries on both sides, but we noted at the end of the simulations beginning traces of stimulated Brillouin backscattering, which remained at a very weak level, and therefore ion dynamics can be ignored in the results we are presenting [This is not logical. Ion dynamics affects SRS saturation by creating IAW mediated LDI and similar instabilities. Given that EPW and KEEN waves live in these simulations, it is incorrect to assume a priori that IAWs could play no role. The only exception to this would be that you ran for a very short time in which case the results are not demonstrative of real situations which occur over 100s of ps at the very least at these intensities]. The initial flat profile of the uniform plasma with the density $n_e = n_i = 1$ (normalized to n) extends over a length $L_p = 1122.56 c / \omega_{pe}$. On either side of the slab the densities are smoothly brought down to zero through a parabolic profile of length $L_{edge} = 7.81 c / \omega_{pe}$. An extra vacuum region of length $L_{vac} = 16.81 c / \omega_{pe}$ exists on each side of the slab, for a total length of the system of $L = 1171.89 c / \omega_{pe}$. In our normalized units $\Delta x = \Delta t$.

A characteristic parameter of laser beams is the normalized vector potential or quiver momentum $|\vec{a}_{\perp}| = |e\vec{A}_{\perp} / M_e c| = a_0$, where $\vec{A}_{\perp}$ is the vector potential of the wave. We chose for the amplitude of the vector potential $a_0 = 0.025$. For the linearly polarized wave

$a_0^2 = I\lambda_0^2 / 1.368 x 10^{18}$, I is the laser intensity in W/cm², and λ_0 the laser wavelength in microns. The frequencies are normalized to the plasma frequency ω_{pe}, and the pump wave frequency ω_0 of the injected laser beam is such that $\omega_0 / \omega_{pe} = 1 / \sqrt{n / n_{cr}}$, which corresponds to $\omega_0 = 3.481$ (normalized to ω_{pe}). Hydrogen ions are used with $M_i / M_e = 1836$. A forward propagating linearly polarized wave is injected in the domain at the left boundary at $x=0$ with $E^+ = 2E_0 \cos(\omega_0 t)$, $E_0 = \omega_0 a_0$ in our units and $E^- = 0$ (no small seed is applied as E^-). (Note that if we choose to normalize time to ω_0^{-1} and length to c / ω_0, then in the results we present in this paper the normalized time and length should be multiplied by ω_0, and the electric field should be divided by ω_0, so that in this case we would have $E_0 = a_0$).

The frequency and wavenumber (ω_0, k_0) of the pump wave are related by the relation $\omega_0^2 = \omega_{pe}^2 + k_0^2 c^2$, or in normalized units $\omega_0^2 = 1 + k_0^2$, from which $k_0 = 3.3343$. For SRS, or the coupling of a pump light wave to a daughter light wave and an electron plasma wave, the values of the electron plasma wavenumber k_{eB} associated with the SRBS, and k_{eF} associated with the SRFS are roots of the equation [32]:

$$\left[(15\Omega / 4 - 6)\right]K^4 + (\mu + 3\Omega - 3)K^2 - 2\mu^{1/2}\left[\Omega^2 - 1 + (5/2\mu)\right]^{1/2}K + 2\Omega - 1 - (5/2\mu)(\Omega - 1) = 0 \quad (15)$$

with $K = k_e \lambda_{De}$ and $\Omega = \omega_0$ (normalized to ω_{pe}). For the present problem we have the following parameters $\mu = m_e c^2 / \kappa T_e = c^2 / v_{te}^2 = 1 / (0.04424\sqrt{T_e})^2 = 255.8$ for $T_e = 2$ keV. The resulting roots are $k_{eB}\lambda_{De} = 0.3377$ for the plasma mode associated with the SRBS, and $k_{eF}\lambda_{De} = 0.0666$ for the plasma mode associated with the SRFS. As discussed in Bers *et al.*, 2009, for these parameters the SRBS plasma wave is heavily damped, and the damping of the SRFS plasma wave is negligible. The heavily damped regime with $k\lambda_{De} > 0.29$ is called the kinetic regime (Kline *et al.*, 2005). In our normalized units the Debye length $\lambda_{De} = v_{te} / c = 0.04424\sqrt{T_e}$ (normalized to c / ω_{pe} in our units), so $\lambda_{De} = 0.06256$ for $T_e = 2$ keV. We finally get $k_{eB} = 0.3377 / \lambda_{De} = 5.398$ for the SRBS plasma wave, and $k_{eF} = 0.0666 / \lambda_{De} = 1.0645$ for the SRFS plasma wave. The corresponding frequencies for the SRBS plasma wave and the SRFS plasma wave are solutions of the equation [32]:

$$\omega^2 \approx 1 + 3k^2\lambda_{De}^2 / \omega^2 + 15k^4\lambda_{De}^4 / \omega^4 - 5/(2\mu) \quad (16)$$

Equation (16) has the following roots: $\omega_{eB} = 1.178$ for the SRBS and $\omega_{eF} = 1.0066$ for the SRFS. The selection rules give the following results for the forward scattered electromagnetic wave (ω_{sF}, k_{sF}) and the backward scattered electromagnetic wave (ω_{sB}, k_{sB}):

$$\omega_{sB} = \omega_0 - \omega_{eB} = 3.481 - 1.178 = 2.303; \quad \omega_{sF} = \omega_0 - \omega_{eF} = 3.481 - 1.0066 = 2.4744 \quad (17)$$

$$k_{sB} = k_{eB} - k_0 = 5.398 - 3.3343 = 2.0637;$$
$$k_{sF} = k_0 - k_{eF} = 3.3343 - 1.0645 = 2.2698$$

(18)

The results in Eqs.(17-18) obey the dispersion relation for the electromagnetic wave: $1 + k_{sF}^2 = 6.152 = \omega_{sF}^2$ (from which we get $\omega_{sF} = 2.480$), and $1 + k_{sB}^2 = 5.2588 = \omega_{sB}^2$ (from which we get 2.293). These results are very close to what is calculated in Eq.(17).

4. Results

We follow the evolution of the system with a close look to the evolution in two regions of the domain, a first one at about a quarter of the length in the domain, and a second one closer to the center of the domain. We will point out important differences in the initial evolution of the spectra between these two regions depending on the level of the round-off errors which now act as a perturbation in the noiseless Vlasov code. So the initial evolution of the SRFS and SRBS is not uniform through the domain, and consequently this affect the initial evolution of the KEEN waves which, as we shall show, develops from the beginning of the Raman scattering.

4.1. Evolution of the system in the first quarter of the length of the plasma domain

For the parameters used in these simulations, the SRFS plasma mode with $k_{eF}\lambda_{De} = 0.0666$ is very weakly damped [32]. No seed or initial perturbation is added to stimulate the heavily damped SRBS mode with $k_{eB}\lambda_{De} = 0.3377$. We present in Figure(1a-2a) and Figure(4,top left) a contour plot of the electron distribution function at a position x between $x \in (280,300)$, at about a quarter of the length of the domain, at a time $t = 351$, 468 and 761 respectively. We see in these figures a modulation with wavelength $\lambda_{eF} = 2\pi / k_{eF} = 5.925$, which is the weakly damped forward scattered mode. Figure (2a) and Figure (4,top left) shows small vortices appearing around $p_{xe} = 0.183$. The phase velocity of the SRBS plasma wave $v_{eB} = \omega_{eB}/k_{eB} = 0.218$, corresponding to a momentum $p_{eB} = v_{eB}\gamma_{eB} = 0.2233$ (where in this case the relativistic factor $\gamma_{eB} = 1/\sqrt{1-v_{eB}^2}$), is different from the position of the observed small vorticities appearing around $p_{xe} = 0.183$ in Fig.(2a) and Figure(4,top left). To identify the spatial modes present in Figures(1a-2a), we present in Figure (1c-2c) the spatial Fourier transform of the longitudinal electric field at the time $t = 351$ and 468 respectively, in the domain $x \in (250,410)$. We identify the dominant mode with $k_{eF} = 1.06$ of the SRFS plasma wave. Since we have a linear polarization, we have in the longitudinal perturbation a mode present with $2k_0 = 6.674$ (at twice the wavenumber of the pump, appearing at 6.676 in our results in Figure (1c)). This is due to the fact that if we have a linearly polarized wave: $\vec{E} = (0, E_y, 0)$, we can write in a linear analysis with $E_y = E_0 \cos(\psi)$, $\psi = (kx - \omega t)$, and Faraday's law is:

$$\frac{\partial \vec{B}}{\partial t} = (0,0,-\frac{\partial E_y}{\partial x}) \tag{19}$$

Then $\vec{B} = (0,0,B_z)$ with $B_z = B_0\cos(\psi)$, and $B_0 = E_0 k/\omega$. From $\vec{E}_\perp = -\partial \vec{a}_\perp/\partial t$ and $\vec{p}_\perp = \vec{a}_\perp$, we get $\vec{p} = (0,p_y,0)$, with $p_y = -p_0\sin(\psi)$, and $p_0 = E_0/\omega$. The longitudinal Lorentz force is $p_y B_z = -\frac{1}{2} k p_0^2 \sin(2\psi)$. This drives a longitudinal response at the 2nd harmonic of the laser wave.

We note in Figs.(1c) a mode with a wavenumber 5.616. These results are confirmed in Figure (3), where we present the spatial Fourier modes at the time t=527 in the same domain $x \in (250,410)$, and where the mode with a wavenumber 5.616 appears with its growing harmonics at 11.232 and 16.81. This mode at k_{KEEN} =5.616 is different from the value of k_{eB} =5.398 for the SRBS plasma wave, and will be further discussed and identified as a KEEN wave, responsible for the small vortices we see in Figure (2a) and Figure (4,top left). We show on a logarithmic scale in Figure (1b) the distribution function around p_{xe}=0.183, spatially averaged over a length λ_{KEEN} =$2\pi/k_{KEEN}$ =1.118 (which is the width of the small vortices we see in Figure (2a) and Figure (4,top left)) around x=280. At this stage at time t=351, it shows on a logarithmic scale the straight line of a Maxwellian. However, in Figure (2b) at time t=468, and in Figure (4,bottom right) at time t=761, the distribution function shows a slightly distorted (but not fully flattened) distribution function, which lower the damping rate and which can facilitate the excitation of the mode around p_{xe}=0.183. The entire distribution function, spatially averaged over a length λ_{KEEN} =1.118 around x=280, is shown at time t=761 in Figure (4,bottom left). Figure (4,top right) shows a plot of the longitudinal electric field in $x \in (280,300)$, showing a wavelength λ_{eF} =$2\pi/k_{eF}$ =5.925 with a small modulation with λ_{KEEN} =1.118.

Figure (5) presents the spatial Fourier spectrum at time t=761 in $x \in (250,410)$. We note in Figure (5a) for the longitudinal wave, the mode with a wavenumber 5.616 has now developed important harmonics at 11.232 and 16.81. We also identify the dominant mode with k_{eF} =1.06 of the SRFS plasma wave. Since we have a linear polarization, we have in the longitudinal perturbation a mode present with $2k_0$ =6.676 (at twice the wavenumber of the pump).

At this stage, we look in Figure (5b) to the wavenumber spectrum of the forward electromagnetic wave E^+ in the domain $x \in (250,410)$. We identify the dominant pump wave, appearing at k_0 =3.338 (3.334 in our theoretical results). We can also identify the contribution of the SRFS plasma wave at k_{sF} =2.277 (2.2698 in our theoretical results in Eq.(18)). We have also a small peak at k_{AS} =4.398, which corresponds to the anti-Stokes coupling $k_{AS} = k_0 + k_{e-AS}$ = 3.334 + 1.064 = 4.398 in our theoretical results (k_{e-AS} =1.064 is the plasma wavenumber for the anti-Stokes coupling, already present in the wide dominant peak k_{eF} =1.06 in Figure (5a)). The frequency ω_{AS} =4.51 of the anti-Stokes wave is calculated from the relation $\omega_{AS}^2 = 1 + k_{AS}^2$, in close agreement with the value calculated from the relation ω_{AS} =
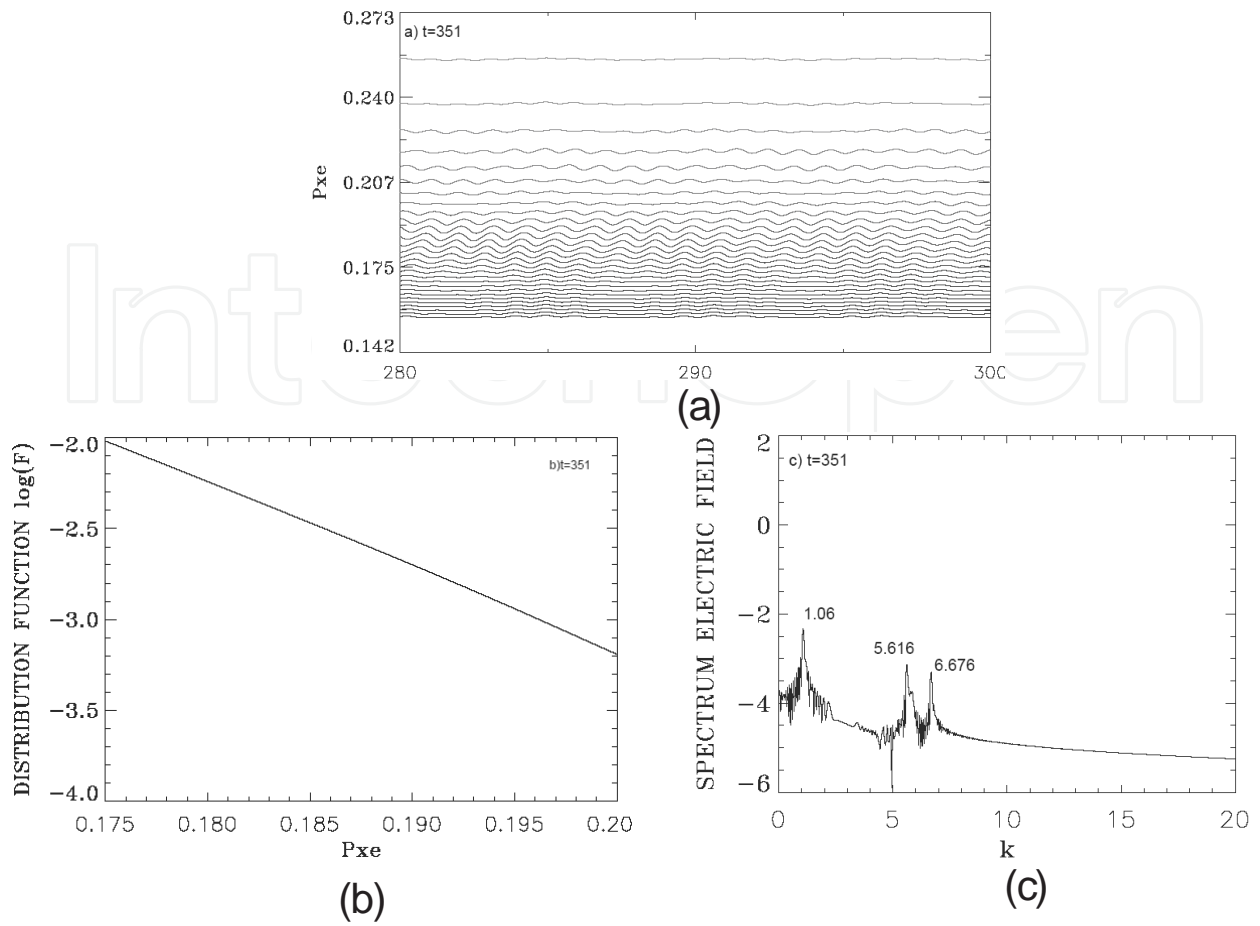
Figure 1. a) Contour plot of the electron distribution function in $x \in (280,300)$ at t=351; b) Distribution function at t=351, spatially averaged around x=280 over a length of $\lambda_{KEEN} = 1.118$; 1c) Spatial Fourier spectrum at time t= 351 in $x \in (250,410)$.
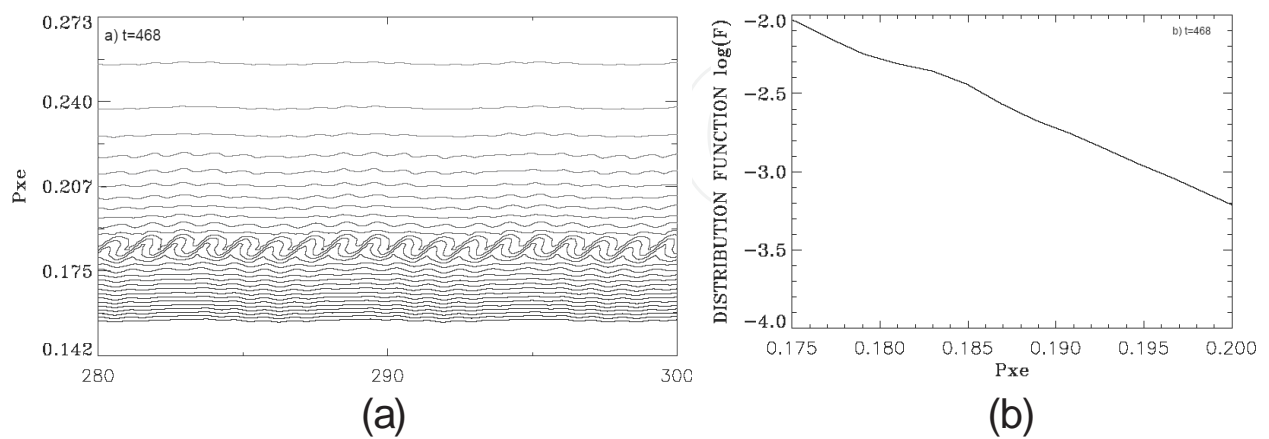
Figure 2. a) Contour plot of the electron distribution function in $x \in (280,300)$ at t=468; b) Distribution function at t=468, spatially averaged around x=280 over a length of $\lambda_{KEEN} = 1.118$

$\omega_0 + \omega_{e-AS} = 3.481 + 1.0066 = 4.487$, where the frequency $\omega_{e-AS} = 1.0066$ associated with the anti-Stokes plasma wave is essentially the same as the already excited SRFS plasma wave at $\omega_{eF} = 1.0066$. These frequencies will be verified when studying the spectrum in Figure (6,7).
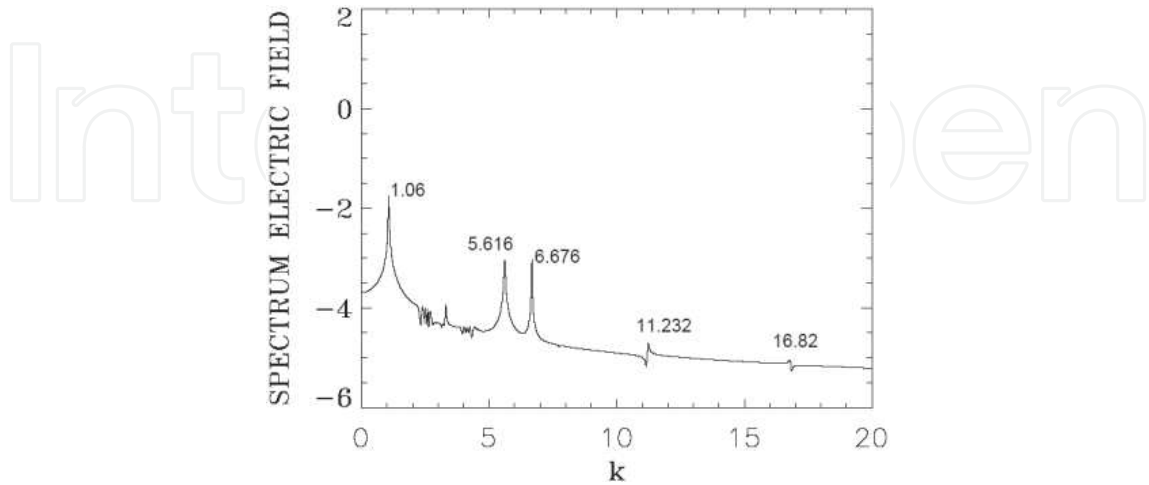
Figure 3. Spatial Fourier spectrum at the time $t=527$ in $x \in (250,410)$

In free space, the forward propagating wave E^+ and the backward propagating wave E^- are strictly decoupled. In a plasma, there is a very weak coupling between E^+ and E^-, due to the nonlinearity of the medium. So the wavenumbers spectrum of E^- in Figure (5c) shows the same peaks at 3.338, 2.2778, 4.398 as in Figure (5b), but at a much lower level (the peak at 4.398 is barely visible, and the peak at 3.338 corresponding to the pump is almost two orders of magnitude smaller in Figure (5c) compared to Figure (5b)), with the exception of the peak at 2.277 which is reaching almost the same level in Figure (5c) as in Figure(5b). This peak of the backward wave at 2.277 in Fig.(5c) couples with the forward direction pump in Figure (5b) at 3.338 to give $k_0 = -k_{sF} + k_{KEEN}$, or a plasma wavenumber $k_{KEEN} = 3.338 + 2.277 = 5.615$ (which is the peak we identified before appearing at 5.616 in Figures (1c,2c,5a)). We have identified this mode as belonging to the KEEN wave (Afeyan *et al.*, 2004 and Afeyan *et al.*, 2013a-f) when discussing above the spectrum. The frequency ω_{KEEN} of this mode verifies $\omega_0 = \omega_{sF} + \omega_{KEEN}$, or $\omega_{KEEN} = 3.481 - 2.474 = 1.007$, and the phase velocity $v_{KEEN} = \omega_{KEEN} / k_{KEEN} = 0.18$, which corresponds to a momentum $p_{KEEN} = v_{KEEN} \gamma_{KEEN} = v_{KEEN} / \sqrt{1 - v_{KEEN}^2} = 0.183$, which is where the small vortices appearing in Figs.(2-4) are located. These vortices are similar to what is presented for instance in references [18-20].

We present in Figure (6a) the frequency spectrum of the forward propagating wave E^+ recorded at the position $x=300$ between $t_1=664$ and $t_2=824$. We identify the pump frequency $\omega_0=3.495$ ($\omega_0=3.481$ in our theoretical results), and two small peaks for the forward scattered mode $\omega_{sF}=2.474$ (see Eq.(17)), and the anti-Stokes mode $\omega_{AS}=4.487=\omega_0+\omega_{e-AS}=3.481+1.0066$. Figure (6b) shows the frequency spectrum of the backward wave E^- at the same position $x=300$, during the same time. It shows the peaks with the forward wave at 3.495 (at much lower level

than in Figure (6a)) and at 2.474 (at essentially the same level as the SRFS mode in Figure (6a)), and a small peak for the weakly growing heavily damped SRBS wave at ω_{sB}=2.28 (2.30 in our theoretical results). So the coupling $\omega_0 = \omega_{sF} + \omega_{KEEN}$, $k_0 = -k_{sF} + k_{KEEN}$ has resulted in an KEEN wave at (ω_{KEEN} =1.007,k_{KEEN} =5.616) which creates the small vortices we see in Figure (2a) and Figure (4a) around p_{KEEN} =0.183, and has resulted in a stimulation of the backward light wave appearing at (ω =2.474,k =2.277) in Figure (6b) and in Figure (5c) respectively. Since the kinetic enhancement of the backward scattering is one of the main point in the investigation of Raman scattering, since it can remove a substantial amount of energy from the pump laser propagating through the plasma, we have here an example of a stimulated backward wave at the wavenumber and frequency of the SRFS wave, which is excited before the SRBS wave through the coupling with the KEEN wave at (ω_{KEEN},k_{KEEN}). The wave at (ω_{KEEN},k_{KEEN}) is trapping a population of electrons at the phase velocity of the wave as in Figure (2a) and in Figure (4a,left). The slope of the distribution function is not flattened at the phase velocity of the KEEN wave, but it is reduced as shown in Figure (4b,right), which allows the wave to be less damped, and to exist and to trap a population of electrons which supports the KEEN wave, and allows it to propagate, as long as the stimulation of the pump is present through the coupling with a backward wave.
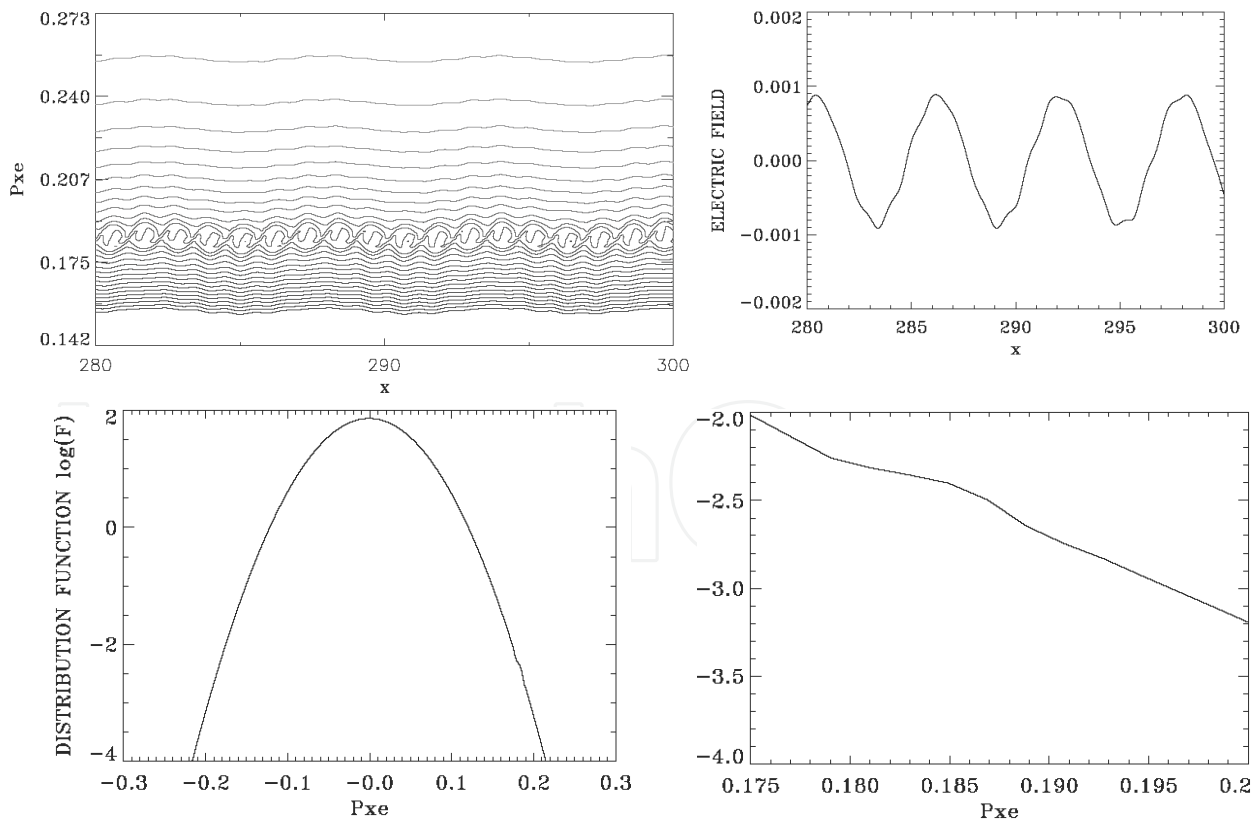
Figure 4. Top left: Contour plot of the electron distribution function in $x \in$ (280,300) at t=761. Top right: Plot of the longitudinal electric field in $x \in$ (280,300). Bottom: Distribution function at t=761, spatially averaged around x=280 over a length of λ_{KEEN} =1.118
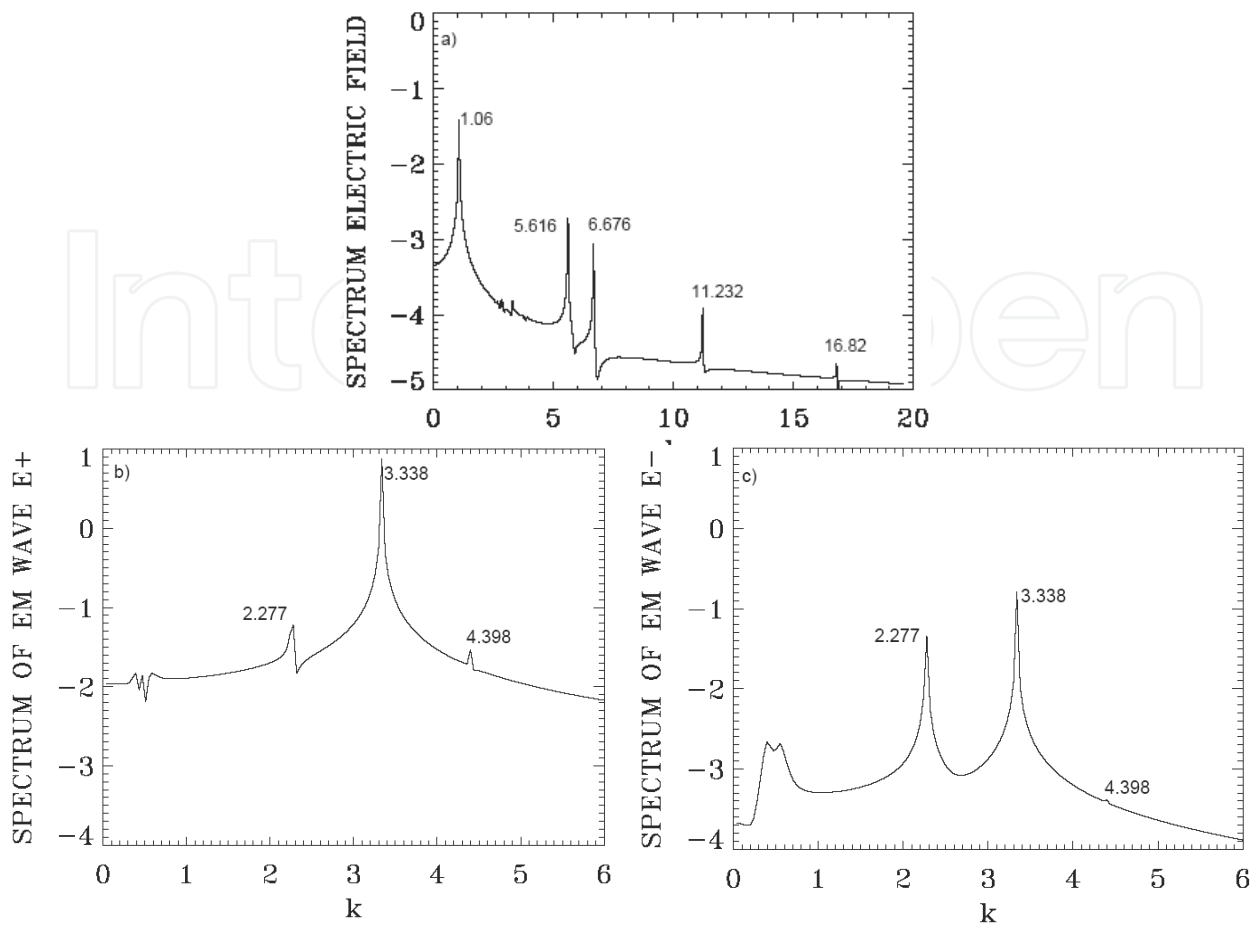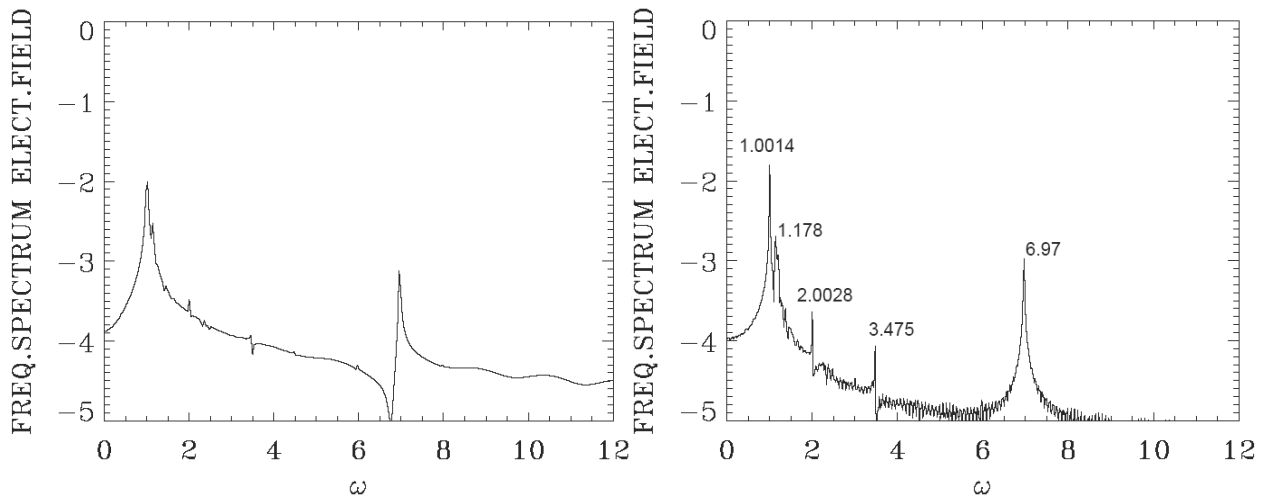
Figure 5. Spatial Fourier spectrum at the time t=761in $x \in (250,410)$ for: a) the longitudinal plasma wave; b) the forward electromagnetic wave E^+; c) the backward electromagnetic wave E^-.
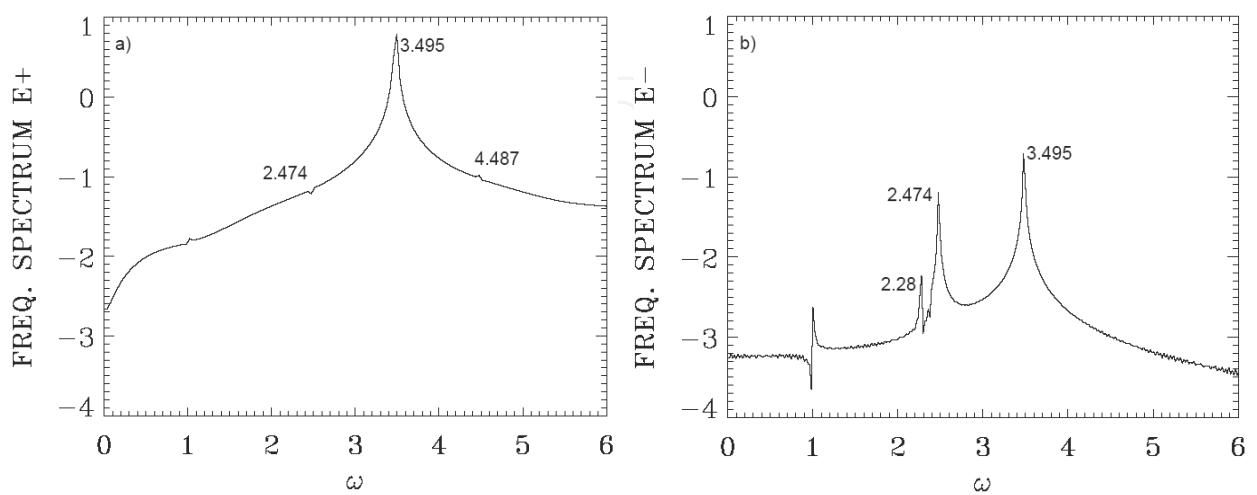
**Figure 6.** Frequency spectrum: a) forward propagating wave E^+; b) backward propagating wave E^-

Figure 7. Frequency spectrum for the longitudinal electric field.

Figure (7,left) shows the frequency spectrum for the longitudinal electric field recorded at the position x=300, during the same time between t_1=664 and t_2=824 as in Figure (6), and Figure (7,right) shows the frequency spectrum at the same position, but between t_1=664 and t_2=984. The comparison emphasizes the growth of the modes present during this phase. We can identify the mode for the SRFS plasma wave ω_{eF} =1.0014 (1.006 in our theoretical results, see Eq.(17), which is also the peak at the KEEN wave ω_{KEEN}), and its harmonic at 2.0028. A smaller peak at 1.178 is for the SRBS plasma wave, heavily damped and which is still slowly growing, appears in Figure (7,right). We also note the mode at the harmonic of the pump $2\omega_0$ = 6.95 (see discussion around Eq.(19)), and its sub-harmonic at the pump frequency ω_0=3.475. In Figure (7), we are still in the phase where the SRFS k_0=k_{sF} + k_{eF} is coupling the pump with the forward scattered wave, and the KEEN wave k_0=$-k_{sF}$ + k_{KEEN} is coupling the pump with the backward wave at $-k_{sF}$, and are dominating, as shown in Figure (4). We can also write $2k_0$=k_{eF} + k_{KEEN}, but $2k_0$= 6.676 is also present in Figure (5a) as the harmonic of the pump as previously explained, further forcing the SKEENS oscillation at k_{KEEN} =5.615 and the SRFS at k_{eF} =1.06.

We have so far shown in this early stage, that the excitation of the KEEN wave and the forward scattering are dominating. We present in Figure (8) the contour plots of the distribution function for $x \in (300,339)$, for t=761, 937 and 966. We see at t=761 in Figure (8a) the same pattern as in Figure (4, top left). However, in Figures (8b,c) we see a mode coming from the right, and propagating to the left while growing, which is the SRBS plasma wave with k_{eB}=5.398 and ω_{eB}=1.178. We will discuss later where and when this mode is generated. Indeed in Figure (7,right), where the frequency spectrum is obtained by extending the time domain from t_1=664 to t_2=984, we see the mode at ω_{eB}=1.178 appearing.

In Figure (9a) we present in the wavenumber spectrum of the longitudinal electric field in the domain $x \in (250,410)$ at t=879 (to be compared with Figure (5a)). We note that the SRBS plasma peak at k_{eB}=5.398 has grown, and eclipsing the KEEN wave peak at k_{KEEN}=5.61. We also see the persistence of the harmonic of the mode k_{KEEN}=5.61 at 11.2. Figure (9c) shows the wavenumber spectrum of the backward wave E^{-}, in the same domain $x \in (250,410)$, at t=879. We see the now growing backscattered wave at k_{sB}=2.08 (2.06 in our theoretical resuls), and the modes at 2.238 and 3.338. The signature of the now growing backscattered wave is seen in the wavenumber spectrum of the forward wave E^{+} in Figure (9b) at k_{sB}=2.05, together with the forward pump at k_0=3.338, the forward scattered wave at k_{sF}=2.2778, and the anti-Stokes mode at k_{AS}=4.398. Figure (10a) shows a contour plot of the distribution function in the domain $x \in (320,339)$ at t=1289, in the final stage close to saturation. Figures (10b) and (10c) shows the spatially averaged distribution function over one wavelength of the SRBS plasma wave, λ_{eB}=2π/k_{eB}=1.16 , which is essentially the width of a vortex in Figure (10a)), at the left edge of the domain in Figure (10b), and in the middle of the domain of Figure (10c) respectively. We see a bump, with a minimum at the phase velocity of the SRBS plasma wave. With k_{eB}=5.398, ω_{eB}=1.178, this corresponds to a phase velocity v_{eB}=ω_{eB}/k_{eB}=0.218, and to a momentum p_{eB}=$v_{eB}\gamma_{eB}$=0.2233, which corresponds to the position of the local minimum we see in Figure (10b) and Figure (10c), and which corresponds also to about the position of the center of the big vortices in Figure (10a).

There is also a local maximum on the bumpy plateau. We look in Figure (11a) to the wavenumber spectrum of the longitudinal electric field at t=1289, close to saturation, in the domain $x \in (250,410)$. We still observe the modes previously discussed, the SRFS plasma wave at k_{eF}=1.06, and the SRBS plasma wave at k_{eB}=5.38 is now dominant, the harmonic of the pump wave at 6.676 is still present, but the modes at 10.799 and 16.18 are harmonics of the now dominant SBRS plasma wave at k_{eB}=5.38 (compare with Figure (5a)). We also see sidebands developing, which is common when positive slopes of the distribution function are formed [33]. Detailed analysis of the eigen-frequencies of the distribution functions with a shape similar to what is presented in Figure (10b) and Figure (10c) has been discussed in details in [22], where BAM and EAW have been identified. The growth of these modes will lead to the fusion of the vortices but they missed KEEN wave contributions and SKEENS processes which we have seen in the SRS physics we present here. Detailed studies at this stage is beyond the scope of the present work, since an accurate study in this case requires a fine grid in velocity space for the proper treatment of the trapped particles effects and of the merging of the vortices. We note however a peak in Figure (11a) at k=4.32. The associated frequency from Eq.(16) is ω=1.11 (we note the broad frequency spectrum in Figure (12a)), which corresponds to a phase velocity v_{φ}=ω/k=0.25, and to a momentum p_{φ}=$v_{\varphi}\gamma$=0.265, which corresponds to the local maximum in the middle of the bumpy plateau. We also have in Fig.(11a) a peak at k=3.33, which corresponds from Eq.(16) to a frequency ω=1.065, and to a phase velocity v_{φ}=ω/k=0.32 and to a momemtum p_{φ}=0.339. This corresponds to the second local minimum we see on the bumpy plateau in Figure (10).
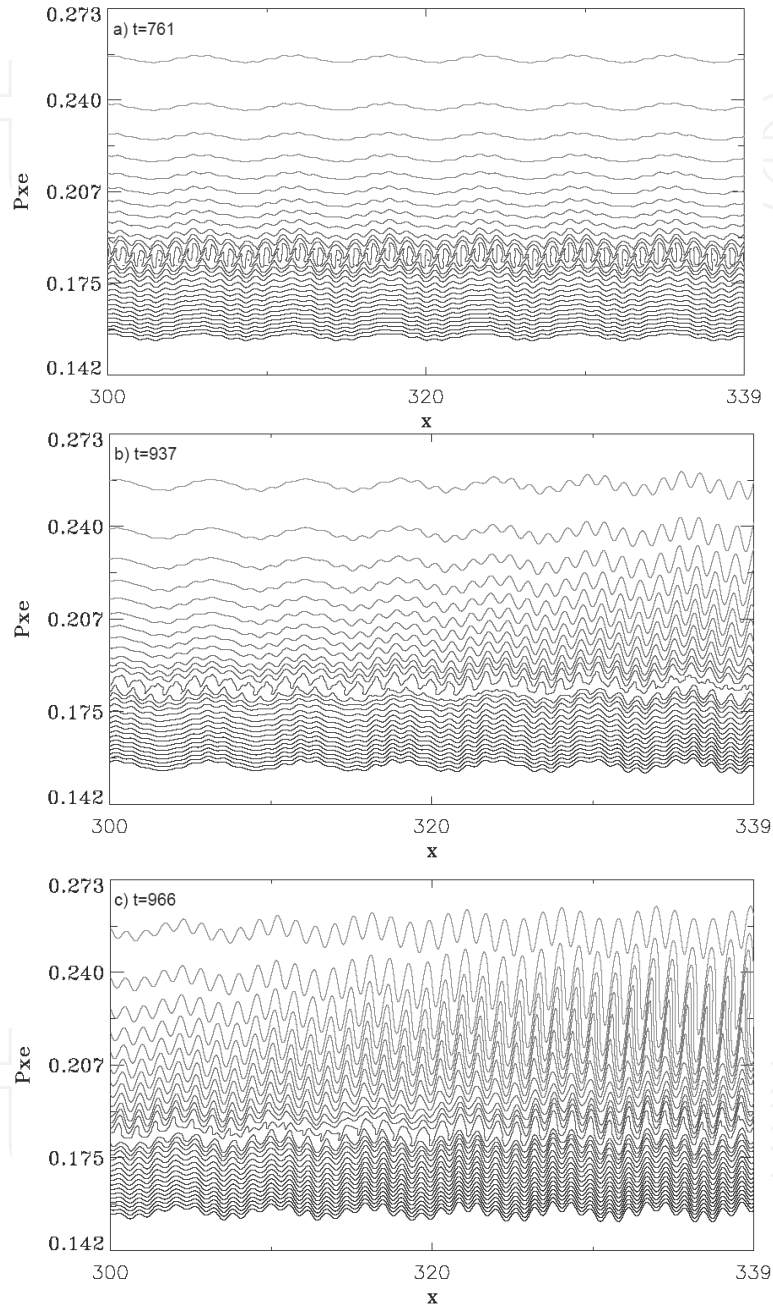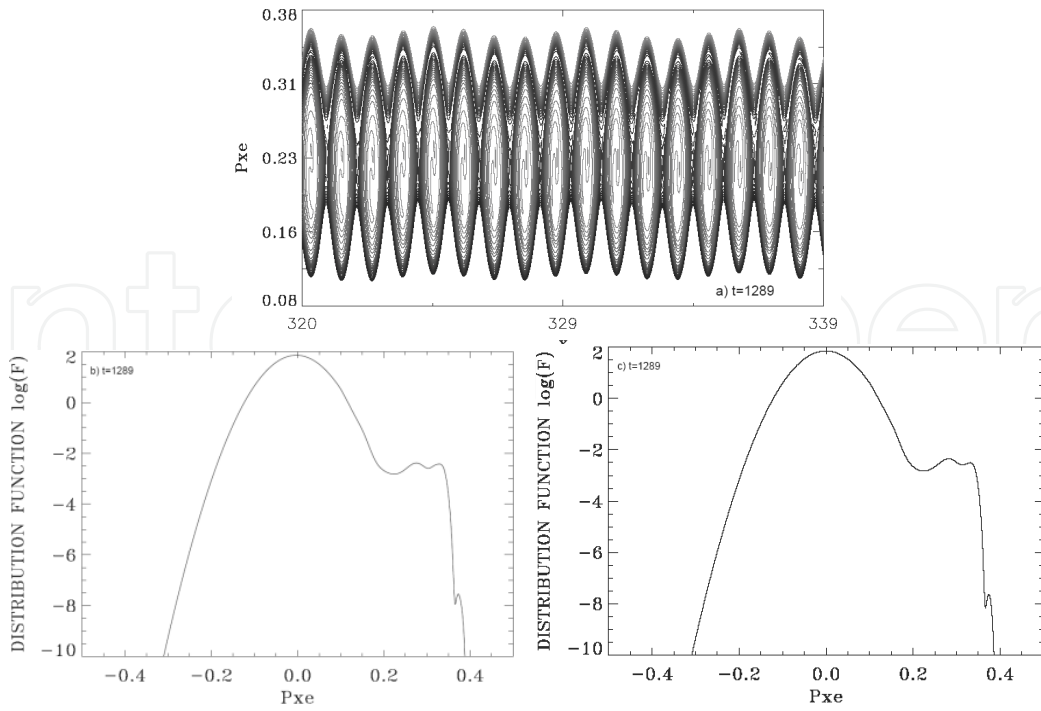
**Figure 8.** Contour plots of the distribution function for $x \in (300,339)$, at: a) t=761; b) t=937; c) t= 966.
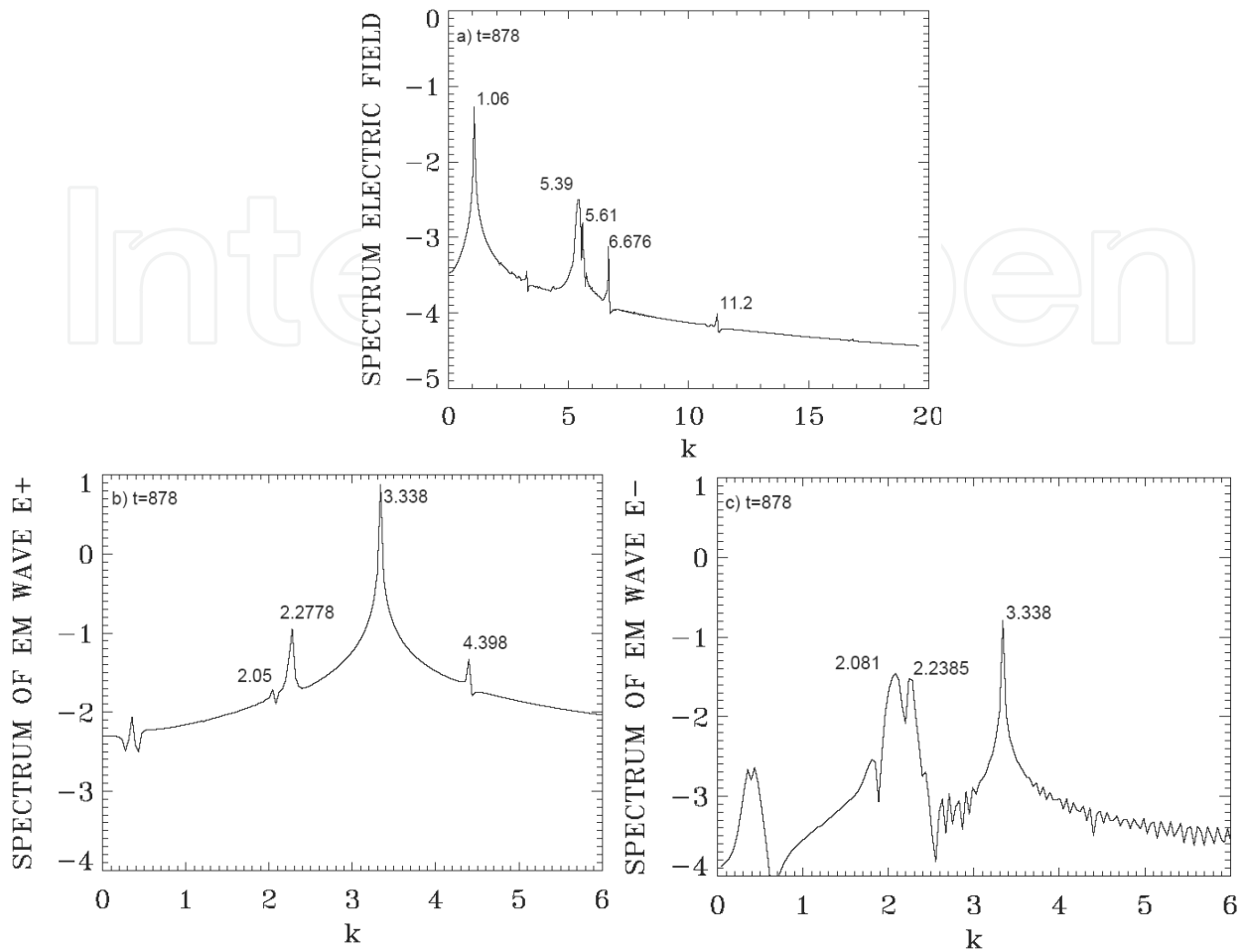
Figure 9. Spatial Fourier spectrum at the time t=878 in $x \in (250,410)$ for: a) the longitudinal plasma wave; b) the forward electromagnetic wave E^+; c) the backward electromagnetic wave E^-.

In Figure (11c) we present the wavenumber spectrum for the backward wave E^- at t= 1289, in the domain $x \in (250,410)$, which shows the now dominant backward mode at k_{sB}=2.042, and a trace of the pump wave at k_0=3.338, and of the anti-Stokes mode at 4.398. And in Figure (11b) we present the spectrum of the forward wave E^+ in the domain $x \in (250,410)$. We see the peak of the pump wave at k_0=3.338. We also see a peak at 2.042 which corresponds to the peak in Figure (11c). We have the peak of the forward scattered mode at k_{sF}=2.277, and the peak for the anti-Stokes k_{AS}=4.398. There is a small peak appearing at 8.718, which grew after the growth of the mode at k_{sB}=2.042 in Figure (11c). We can write 8.718= 10.8-2.042 (k_{sB}=2.042) or 8.718=6.676+2.042, which also happens to be at the harmonic of the anti-Stokes at 4.398. These results belong to the further evolution of the nonlinear stage which is beyond the scope of this work.

**Figure 10.** At *t*=1289: a) contour plot of the distribution function in the domain $x \in (320,339)$; b) averaged distribution function at *x*=320; c) averaged distribution function at *x*=329.
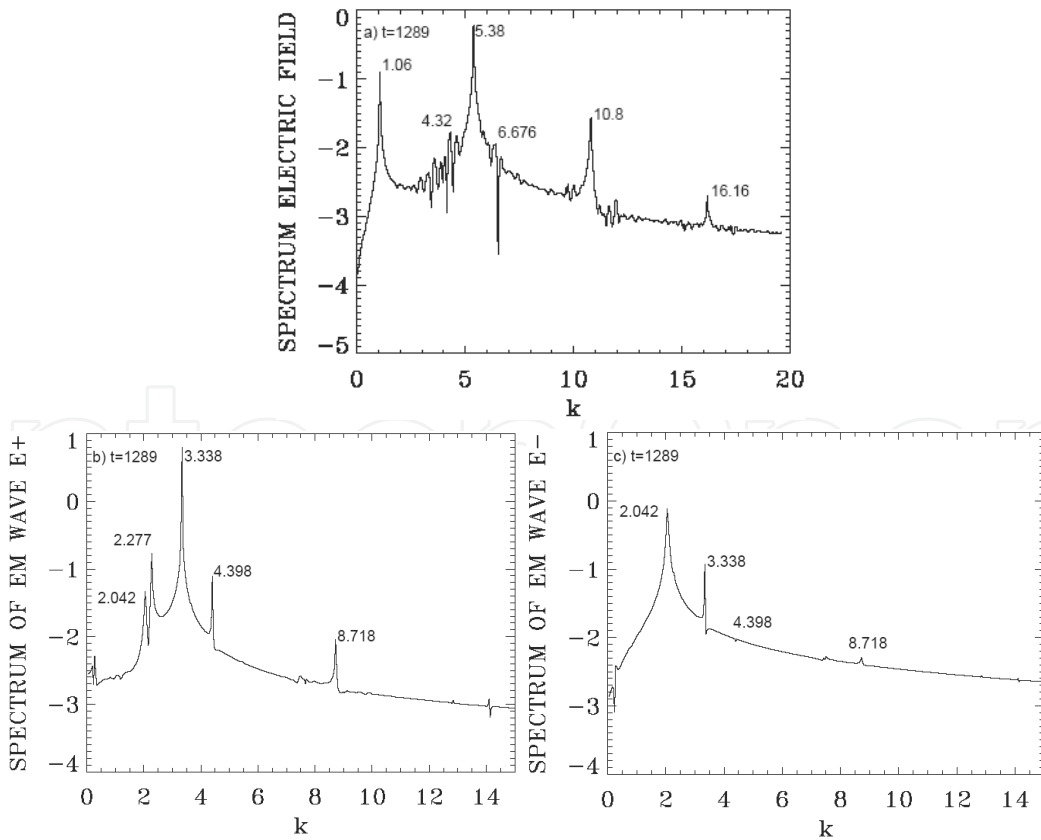
Figure 11. Spatial Fourier spectrum at the time *t*=1289 in $x \in (250,410)$ for: a) the longitudinal plasma wave; b) the forward electromagnetic wave E^+; c) the backward electromagnetic wave E^-.

We present in Figure (12) the frequency spectra between t_1=1132 and t_2=1292, at the position x=300. The dominant peak in Figure (12a) is now for the SRBS plasma wave at ω_{eB}=1.178. However, this peak is broad and includes peaks at 1.006 of the SRFS plasma wave ω_{eF} and the KEEN wave ω_{KEEN}. The other peaks are at 2.356, 3.534 (these peaks are very close to second and third harmonic of the now dominant SRBS plasma wave at ω_{eB}=1.178). We have also a peak at 4.55, and the peak at the harmonic of the pump at $2\omega_0$= 6.951. In Figure (12c) we see the now dominant backward mode at ω_{sB}=2.277, and the trace of the pump at 3.495. The trace of the anti-Stokes mode is negligible. In Figure (12b) we identify the pump wave in the forward direction at ω_0=3.495, and the trace of the backward wave at 2.277. The anti-Stokes peak at ω_{AS}=4.487 appears negligible. The broad spectrum at 2.277 in Figure (12b,c) would also include the SRFS peak at 2.474.
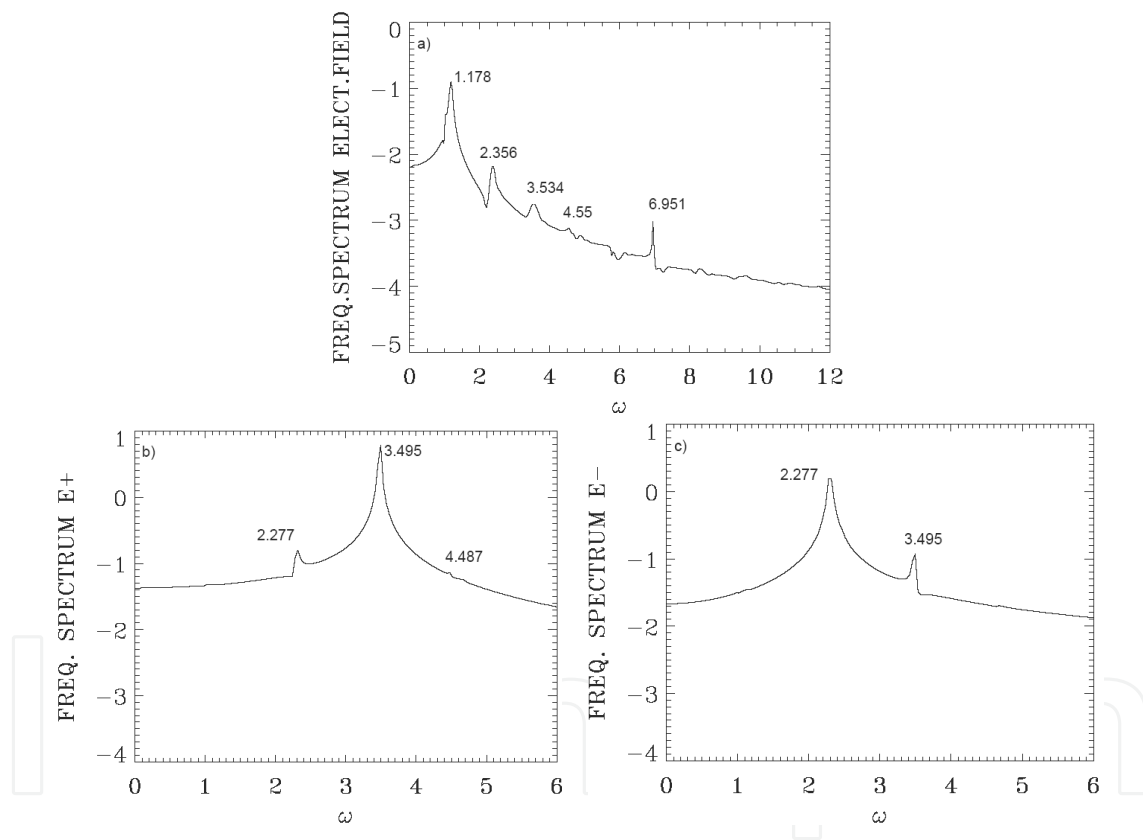

Figure 12. Frequency spectrum recorded at x=300, between t_1=1132 and t_2=1292 : a) longitudinal plasma wave; b) forward propagating wave E^+; c) backward propagating wave E^-

4.2. Evolution of the system around the center of the domain

We present in Figure (13) a plot of the longitudinal electric field at t=761 (at the time we present the spectrum in Figure (5), after about 39000 time steps). The maximum of the electric field in Figure (13) is between x=400 or x=500. We look in Figure (14) to the phase-space contour plot
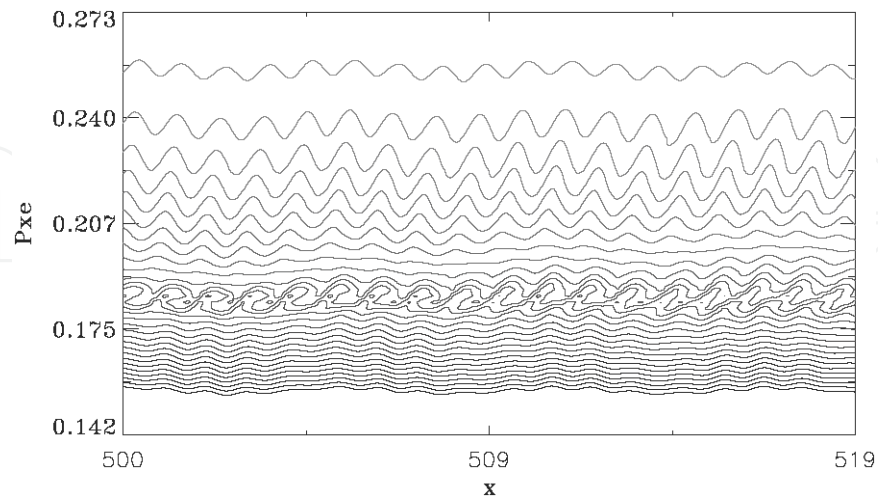
of the electron distribution function in $x \in (500,519)$. We see the small vortices of the KEEN wave similar to what has been presented and discussed in Figure (4) at the same time. However, Figure (14) shows the presence of the growing SRBS plasma wave absent from Figure (4). The reason is that at that time, the round-off errors in the region around $x=400$ or $x=500$ have reached a sufficiently high level to act as a perturbation, which stimulates the growth of the SRBS plasma wave, at the same time as the SKEENS we have identified and studied in section 4.1.
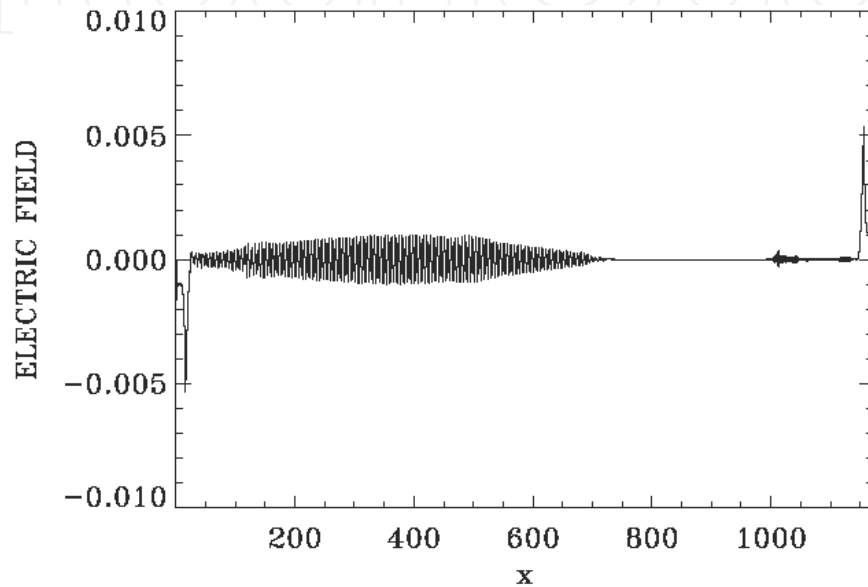
Figure 13. Plot of the longitudinal electric field at t=761.

In Figure (15) we present in the domain $x \in (380,619)$, at t=820, the phase-space contour plots of the electron distribution function. We note the rapid growth of the SRBS plasma wave, in addition to the SKEENS. We observe in Figures (15a,b) the same pattern as in Figures.(8a,b). In Figure (15a), we see the dominant modes excited are the SRFS plasma wave with $k_{eF} = 1.0645$ (wavelength λ_{sF} =5.9), and the KEEN wave associated with the small vortices with k_{KEEN} =5.616 (with a wavelength λ_{eA} =1.118). These small vortices have a phase velocity $v_{KEEN} = \omega_{KEEN}/k_{KEEN}$ =0.18, which corresponds to a momentum $p_{KEEN} = v_{KEEN}/\sqrt{1-v_{KEEN}^2}$ =0.183, as previously discussed for Figure (4,top left). Again these vortices are similar to what is presented in [18] for ponderomotively driven KEEN waves (see also [19-20]). Figure (15b) shows the SRBS plasma wave with k_{eB} =5.39 propagating from right to left. If we follow the different frames in Figure (15), we see that the heavily damped SRBS plasma wave with k_{eB} =5.39 seems to have been excited around x=500, at a time and position where it is stimulated by the now substantial level reached by the round-off errors. From this position, the excited SRBS plasma wave will propagate to the left and to the right, as in Figure (15), excited by the round-off errors perturbation, which now are growing to the left and to the right around x=500. It is this

backward propagating plasma wave that we see appearing in the domain $x \in (300,339)$ in Figures (8b,c).

Figure 14. Phase-space contour plot of the electron distribution function in $x \in (500,519)$, att=761.

So the pattern of excitation of the modes to the right of the domain, for instance in $x \in (460,619)$ in Figure (15) is now different from what has been observed to the left, in $x \in (380,520)$ in Figure (15) for instance or in Figure (4, top left). The wavenumber spectrum for the longitudinal electric field in the domain $x \in (400,560)$ at t=820, during the period of the growth, is given in Figure (16). It shows similar peaks as in Figure (5a), with the exception that now the SBRS plasma wave at k_{eB}=5.38 dominates with respect to the KEEN wave peak at 5.61, with its harmonics at 11.27 and 16.77. The wavenumber spectrum of the backward wave E^-, shows a peak of the backward scattered wave with k_{sB}=2.042, ($k_0 = -k_{sB} + k_{eB}$) much higher than the peak of the wave at 2.277 (compare with Figure (5c)). We also have peaks at 3.338 and 4.398, excited by the coupling with the modes with the same wavenumbers for the forward mode pump with k_0=3.338, and the small peak at 4.398 for the anti-Stokes wave (similar to what has been discussed for Figure(5)). The frequency spectra shows the frequencies of the growing modes, close to what we observe in Figures (6,7). A more complete description of the spectra is given in the end.

Figure (17) shows the longitudinal electric field profile at t=1289. We finally present in Figures (18,19) the wavenumber and frequency spectra at t=1289, at the end of the simulation, in the domain $x \in (400,560)$. Figure (18) should be compared to Figure (11). We still observe the modes previously discussed, the SRFS plasma wave at k_{eF}=1.06, the now dominant SRBS plasma wave at k_{eB}=5.39, the harmonic of the pump wave at $2\omega_0$=6.676, and the harmonics of the now dominant SRBS plasma mode k_{eB} at 10.799 and 16.18. We also see sidebands developing, which is common when positive slopes of the distribution function are formed [33].
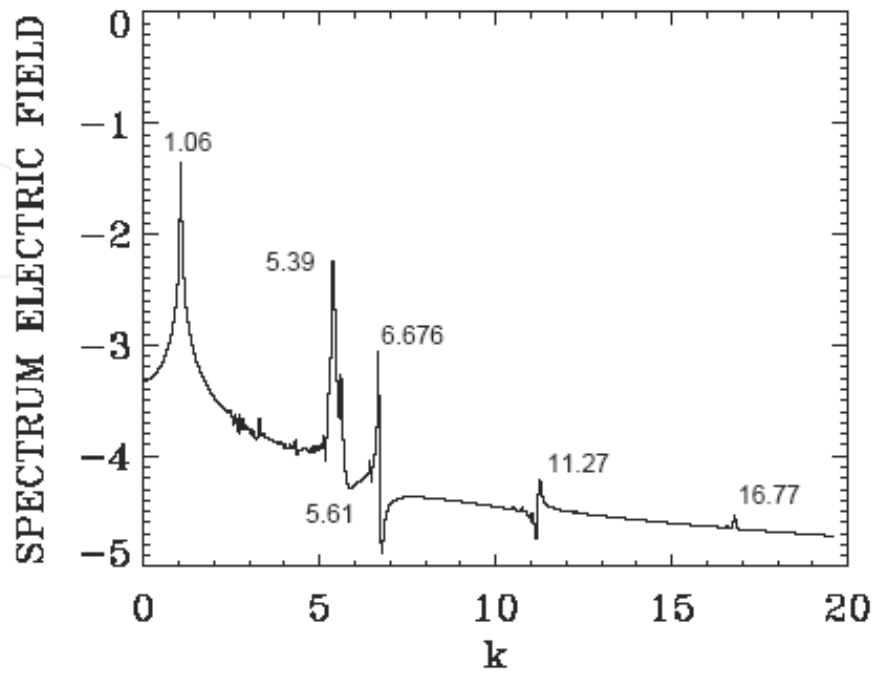
In Figure (18b,c) we present the wavenumber spectrum of the longitudinal electric field, the forward wave E^+ and the backward wave E^-, toward the end of the simulation at t= 1289, in
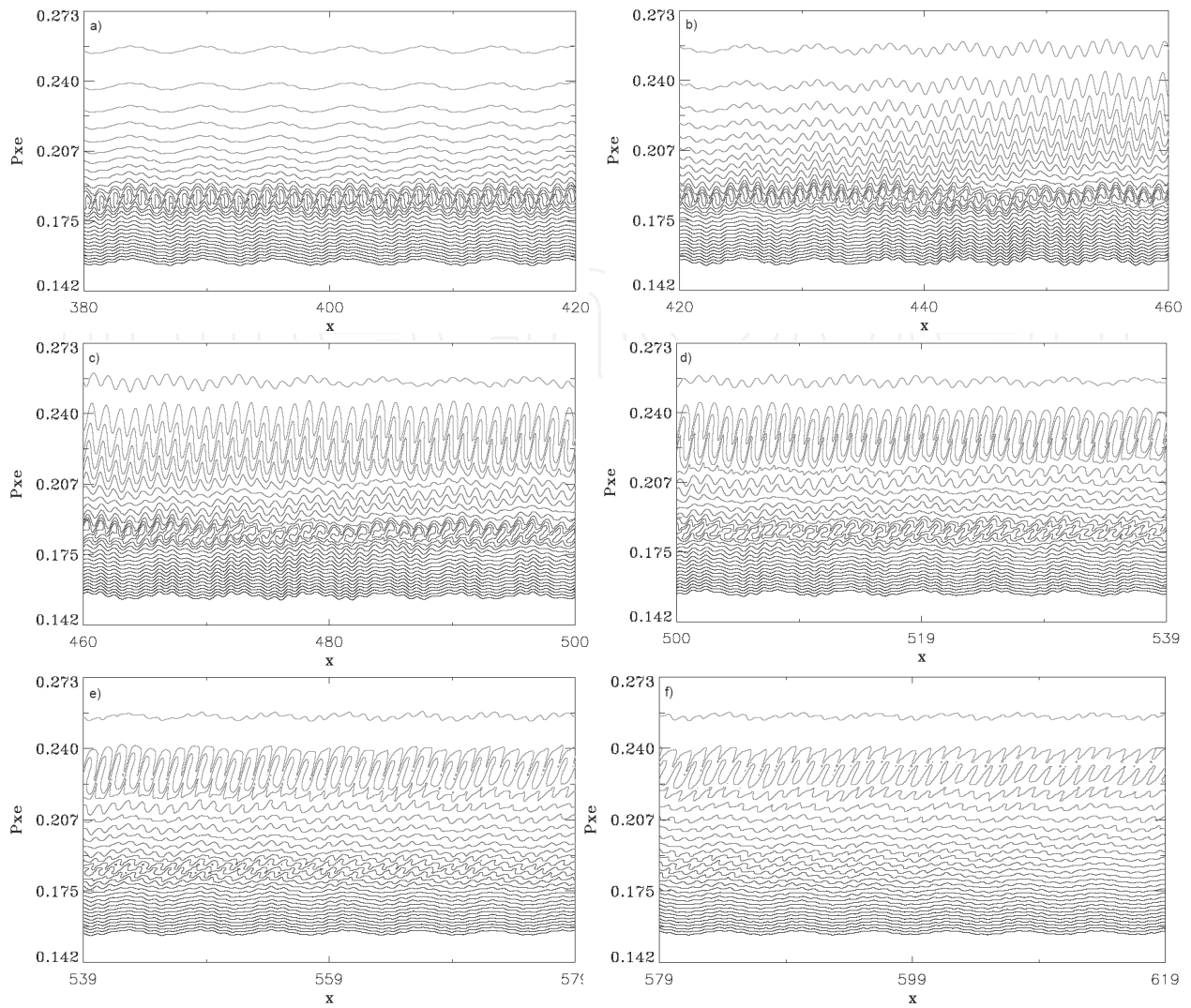
Figure 15. Phase-space contour plot of the electron distribution function in $x \in (380,619)$ at t=820.

the domain $x \in (400,560)$. We see in Figure (18c) for the wavenumber spectrum for the backward wave E^- the dominant backward mode at k_{sB}=2.042, and the trace of the pump wave at k_0=3.338. We see a small peak of the forward scattered mode at 2.277 which corresponds to the peak in Figure (18b). We also see in Figure (18b) the peak of the forward scattered mode at k_{sF} =2.277, the peak for the anti-Stokes k_{AS} =4.3985, and the peak of the pump at k_0=3.338. The small peak at 2.042 corresponds to the dominant backward mode at k_{sB}=2.042 in Figure (18c). There is a small peak at 8.718 which grew after the growth of the mode at k_{sB}=2.042 in Figure (18c). This mode can be the result of a forced oscillation. We can write 8.7= 10.76-2.042 (k_{sB}=2.042), which is a coupling with the harmonic of the SRBS plasma wave at $2k_{eB}$=10.78, or 8.718=6.676+2.042, which involves a coupling with $2k_0$=6.676 (the plasma wave excited at the harmonic of the pump). Note also that the mode at 8.718 is close to the harmonic of the anti-Stokes excited at 4.398.
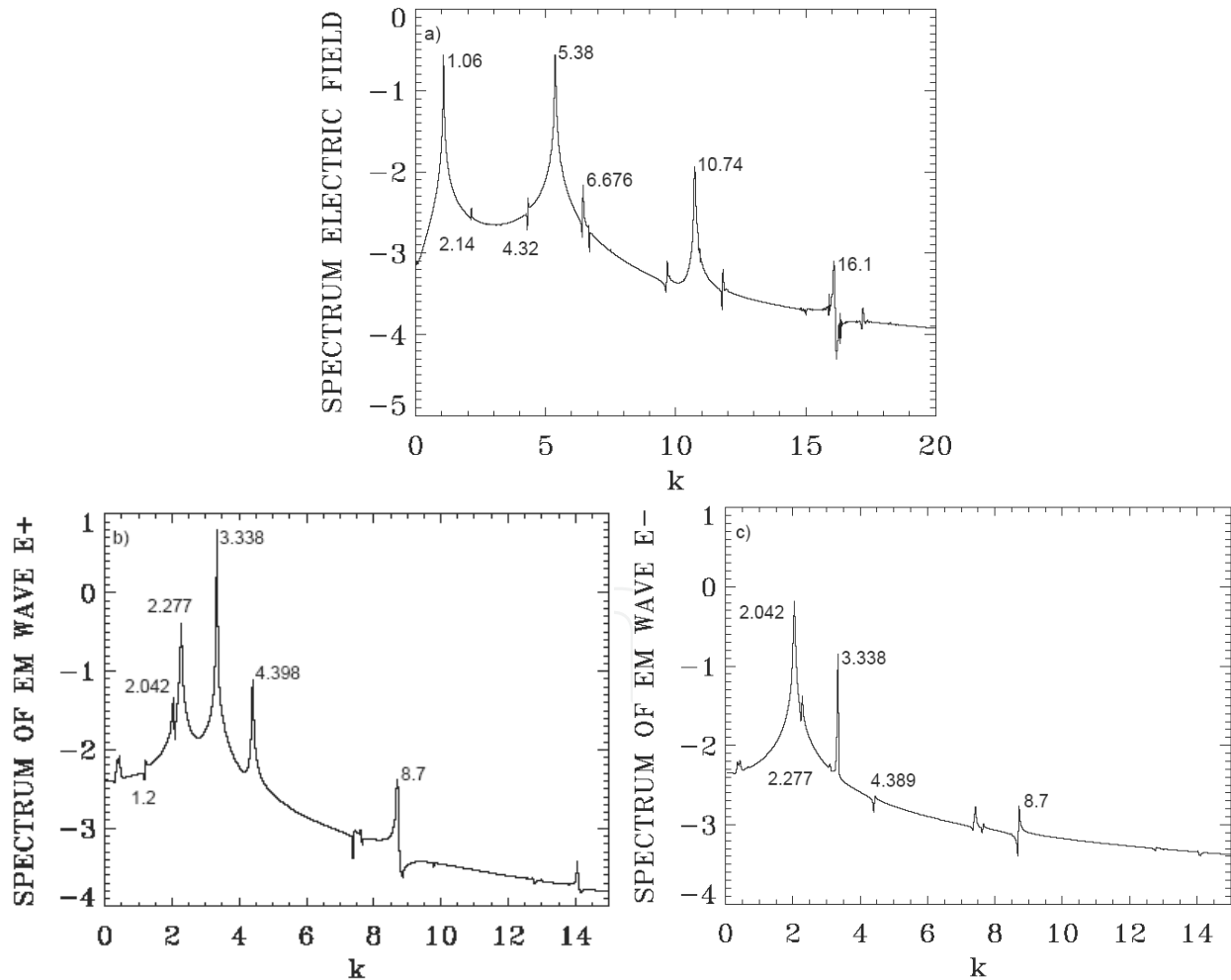
Figure 16. The wavenumber spectrum in the domain $x \in (400,560)$ at t=820, for the longitudinal electric field.
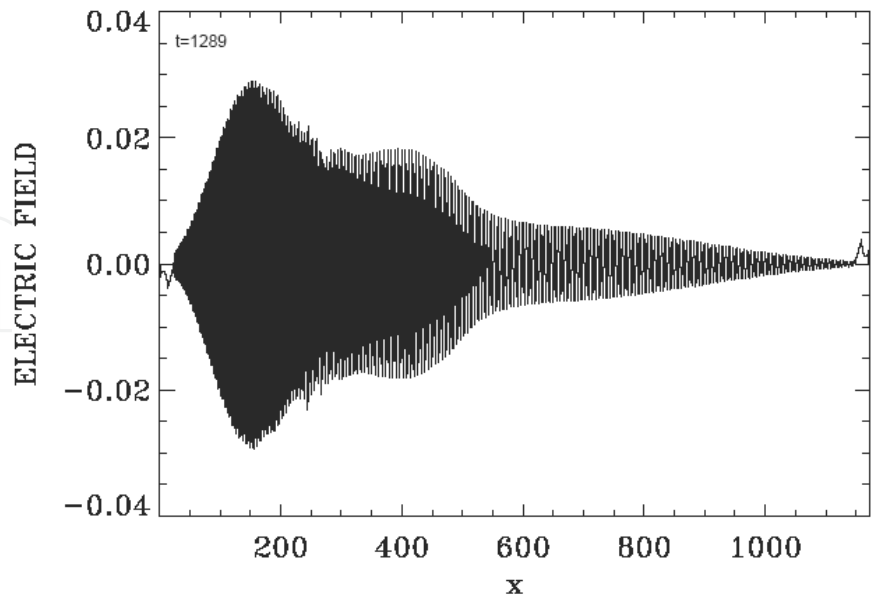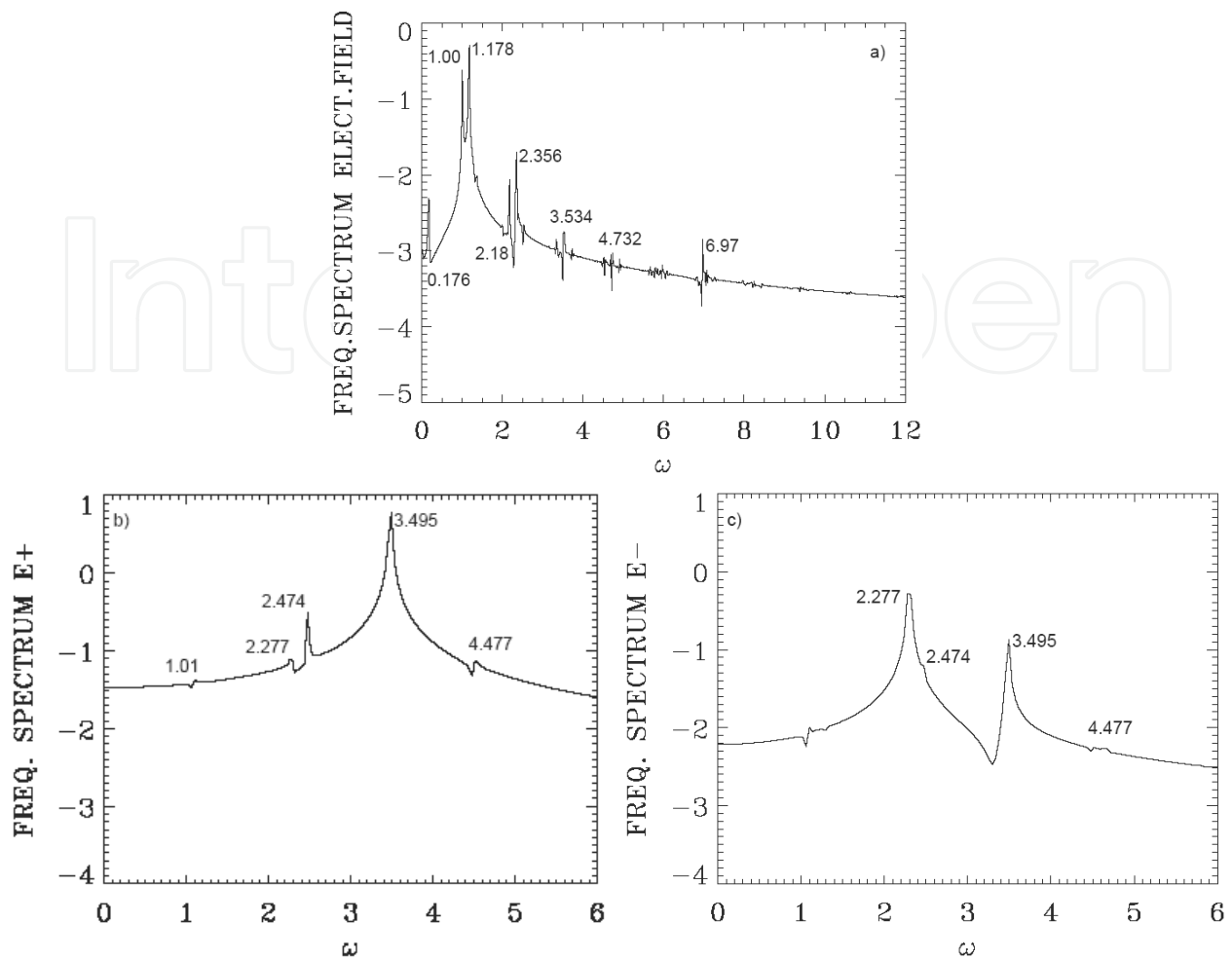

Figure 17. Longitudinal electric field profile at t=1289.

To identify the frequency spectra at the end of the simulation, we present in Figure (19) the frequency spectra between t_1=1113 and t_2=1273, at the position x=450. We identify in Fig. (19a) the local peak at ω_{eF} =1.0014 of the SRFS plasma wave (1.006 in our theoretical value). The dominant peak is for the SRBS plasma wave at ω_{eB}=1.178. The other peaks are at 0.1767, 2.18, and 2.356, 3.534, 4.732 (these last three very close to second, third harmonic and fourth harmonic of ω_{eB}=1.178). We have also a peak at the harmonic of the pump $2\omega_0$= 6.951. In Fig. (19c) we see the now dominant backward scattered mode at ω_{sB}=2.277, and the trace of the pump at 3.495. The trace of the anti-Stokes is negligible. In Figure (19b) we see the pump wave, dominant in the forward direction, at ω_0=3.495, and the trace of the backward wave at 2.277. We see also the forward scattered mode at 2.474. The anti-Stokes peak at ω_{AS} =4.487 appears negligible. In our normalized units (velocity normalized to the velocity of light) v_T/c=0.06256 at T_e=2keV. With ω =0.176, we get k =2.169, very close to the peak at 2.14 in Figure (18a), which is close to the harmonic of 1.06 in Figure (18a).

Figure 18. The wavenumber spectra in the domain $x \in (400,560)$ at t=1289, for: a) the longitudinal electric field; b) the forward propagating wave E^+; c) the backward propagating wave E^-.

Figure 19. Frequency spectra recorded at the position $x=450$, between $t_1=1113$ and $t_2=1273$ for: a) the longitudinal electric field; b) the forward propagating wave E^+; c) the backward propagating wave E^-.

5. Conclusion

In laser fusion, the coupling and propagation of the laser beams in the plasma surrounding the pellet can be the scene of nonlinear processes such as parametric instabilities, which must be well understood and controlled to keep them at low levels, since they are detrimental to laser fusion because they can lead to losses of energy and illumination uniformity. Recent publications [22,23,34-40] have identified the need for a deeper understanding of laser-plasma interactions, and the importance of a kinetic treatment of the plasma, particularly in the regimes currently being approached by the new generation of lasers, and for the treatment of modes such as KEEN waves [18-20], even newer horizons are opened up. The old picture of EPWs and their evolution is now replaced by a much richer scenario of multiple harmonic waves transiently trapping, untrapping and retrapping paricle distributions that maintain the wave on average but without the need for flat distribution functions as in the canonical BGK mode setting of lore.

We showed for the first time in this study that a seemless transition occurs from Raman forward scatter, to the standing wave excited KEEN wave very near the backscattering plasma wave so that the distribution function is strongly modified by the KEEN wave before the EPW can be excited in SRBS. For the parameters we have investigated, the SRBS process is preceded by KEEN waves and then competes with SKEENS for supremacy and eventual merging. This rich physics was not observed when strong seeding of the backscattered wave prevented any detection of these intermediate processes.

The accurate representation and evolution of the particles distribution function provided by the Eulerian Vlasov code offers a powerful tool to study highly nonlinear nonstationary processes in high energy density plasmas. We have uncovered some distinctive features of KEEN waves participating in the Raman process, using a 1D Eulerian Vlasov-Maxwell code that relativistically evolves both ions and electrons. To avoid any interference from artificially distorted distribution functions or imposed linear wave seeding, we start the code from an initial Maxwellian distribution, and a very weak scattered light field standing wave pattern which is enough to trigger both SRFS and then SKEENS. The system evolves under the influence of a pump light wave which provides fluctuations from which SRBS eventually develops. We identify in the early phase of the Raman interaction a reflected light that matches the backscattering of the pump laser off a KEEN wave whose fundamental harmonic has the same wavelength as the forward scattered light, and its appearance precedes the growth and saturation of SRBS. The evolution of the system is however modified with the results presented in section 4.2, close to the center of the simulation domain. In this region, the round-off errors have reached a level where they act as a perturbation, leading to the simultaneous appearance and growth of the SRBS process, in addition to the KEEN wave (see Figure (14)). So we have two distinct evolution scenarios of Raman scattering in the domain we study. To the right of the region $x \in (500,519)$ in Figure (14), we see a simultaneous growth of the SRBS plasma wave and the KEEN wave (see Figure (15)). And to the left of the region $x \in (500,519)$, the growth of the round-off errors acting as a perturbation leads to the appearance of SRBS plasma waves moving to the left in the backward direction. This is where the KEEN wave has already reached saturation, causing heating and relative flattening of the electron distribution function, which shows a structure with a trapped population of electrons. Note the harmonic structure associated with the SRBS mode ω_{eB}=1.178, k_{eB}=5.38 in Figures (11a,12a). Recent publications have pointed to the importance of 2D and 3D effects for a rigorous theory of SRS saturation [41]. This is beyond the scope of the present work. We have restricted our study to the initial phase of the evolution of Raman scattering, and we have shown that in this case scattering off a KEEN wave can produce a backward wave which contributes to the inflation of the Raman signal well before the SRBS starts growing on its own.

In future studies, we propose to investigate the physics of the interaction between SKEENS and SRBS, but eliminating the need for SRFS initiation. This can be achieved by driving the KEEN wave directly by the ponderomotive force generated by the beating of the pump and the appropriate seed electromagnetic wave. Driving KEEN waves directly and electromagnetically generalizes the work of Afeyan et al. [18-20] which has been based on the Vlasov-

Poisson system of equations. We expect to find interesting resonances, even with KEEN waves that have significantly lower phase velocities than the electron plasma waves. The work here showed the coevolution of SKEENS and SRBS for electrostatic waves whose phase velocities were so close that their vortical structures in phase-space directly overlapped and were eventually mixed.

Acknowledgements

Author details

Magdi Shoucri[1] and Bedros Afeyan[2]

1 Institut de recherche Hydro-Québec (IREQ), Varennes, Québec, Canada

2 Polymath Research Inc., Pleasanton, CA, USA

References

[1]   Atzeni S, Meyer-ter-Vehn J. The Physics of Inertial Fusion. Oxford; 2004.

[2]   Kruer W L. The Physics of Laser Plasma Interactions. Westview; 2003.

[3]   Afeyan B, Williams E A. Variational Approach to Parametric Instabilities in Inhomogeneous Plasmas I: Two Model Problems. Phys. Plasmas 1997; 4, 3788.

[4]   Afeyan B, Williams E A. Variational Approach to Parametric Instabilities in Inhomogeneous Plasmas II: Stimulated Raman Scattering. Phys. Plasmas 1997; 4, 3803.

[5]   Afeyan B, Williams E A. Variational Approach to Parametric Instabilities in Inhomogeneous Plasmas III: Two-Plasmon Decay. Phys. Plasmas 1997; 4, 3827.

[6]   Afeyan B, Williams E.A. Variational Approach to Parametric Instabilities in Inhomogeneous Plasmas IV: The mixed polarization high-frequency instability. Phys. Plasmas 1997; 4, 3845.

[7]   Kono M, Skoric M M. Nonlinear Physics of Plasmas. Springer; 2010

[8]   Sagdeev R Z, Galeev A A. Nonlinear Plasma Theory. W. A. Benjamin; 1969

[9]   Davidson D C. Methods of Nonlinear Plasma Theory. Academic Press; 1972

[10]   Elskens Y, Escande D. Microscopic Dynamics of Plasmas and Chaos. IoP; 2003

[11]   Shoucri M. Numerical Simulation of Intense Laser-Plasma Interaction using an Euler-ian Vlasov Code. Proc. 34th EPS Conf. Plasma Phys., Warsaw. ECA Vol. 31F, P-2.007; 2007

[12]   Shoucri M. Numerical Solution of Hyperbolic Differential Equations. New York: No-va Science Publishers; 2008

[13]   Shoucri M. Numerical Simulation of Wake-Field Acceleration Using an Eulerian Vla-sov Code. Commun. Comp. Phys. 2008; 4, 703-718

[14]   Shoucri M. The application of the Method of Characteristics for the Numerical Solu-tion of Hyperbolic Differential Equations. In: Numerical Simulation Research Prog-ress. S.P. Colombo & C.L. Rizzo (Ed.). New York: Nova Science Publishers; 2009

[15]   Shoucri M. Numerical Solution of the Relativistic Vlasov-Maxwell Equations for the Study of the interaction of a High Intensity Laser Beam Normally Incident on an Overdense Plasma. In: Eulerian Codes for the Numerical Solution of the Kinetic Equations of Plasmas. M. Shoucri (Ed.). New York: Nova Science Publishers; 2011

[16]   Shoucri M. Ion Acceleration and Plasma JET Formation in the Interaction of an In-tense Laser Beam Normally Incident on an Overdense Plasma: a Vlasov Code Simu-lation. Comp. Sci. Disc. 2012; 5, 014005/1-19

[17]   Cordier S, Goudon Th, Gutnic M, Sonnendrucker E. Numerical Methods for Hyper-bolic and Kinetic Problems. European Mathematical Society; 2005

[18]   Afeyan B et al. Kinetic Electrostatic Electron Nonlinear (KEEN) Waves and their In-teractions Driven by the Ponderomotive force of crossing laser beams. Proc. Interna-tional Fusion Sciences and Applications. B Hammel, D Meyerhofer, J. Meyer-ter-Vehn, H Azechi (Eds.). American Nuclear Society, pp. 213. arXiv:1210.8105; 2004

[19]   Afeyan B, Charbonneau-Lefort M, Won K, Savchenko V, Shoucri M. The Generation of Self-Organization of Ponderomotively Driven Kinetic Electrostatic Electron Non-linear (KEEN) Waves in High Energy Density Plasmas. To be submitted to Phys. Rev. Lett. 2014

[20]   Afeyan B, Dodhy A, Mehrenberger M., Sonnendrucker E. Long Time Evolution of KEEN Waves Excited with Low Levels Ponderomotive Drive. To be submitted to Phys. Rev. E 2014

[21]   Strozzi D J, Shoucri M M, Bers A, Williams E A, Langdon A B. Vlasov Simulations of Trapping and Inhomogeneity in Raman Scattering. J. Plasma Phys. 2006; 72, 1299-1302

[22] Strozzi D J, Williams E A, Langdon A B, Bers A. Kinetic Enhancement of Raman Backscatter, and Electron Acoustic Thomson Scatter. Phys. Plasmas 2007; 14, 013104/1-13

[23] Strozzi D J, Williams E A, Langdon A B, Bers A, Brunner S. Eulerian-Lagrangian Kinetic Simulations of Laser-Plasma Interactions. In: Eulerian Codes for the Numerical Solution of the Kinetic Equations of Plasmas. M. Shoucri (Ed.). New York: Nova Science Publishers; 2010

[24] Yin L, Daughton W, Albright B J, Bezerrides B, DuBois D F, Kindel J M,Vu H X. Nonlinear Development of Stimulated Raman Scattering from Electrostatic Modes Excited by Self-Consistent non-Maxwellian Velocity Distribution. Phys. Rev. E 2006; 73, 025401/1-4

[25] Vu H X, Yin L, DuBois D F, Bezzerides B, Dodd E S. Nonlinear, Spectral Signatures and Spatiotemporal Behavior of Stimulated Raman Scattering from Single Laser Speckles. Phys. Rev. Lett. 2005; 95, 245003/1-4

[26] Montgomery D S, Focia R J, Rose H A, Russel D A, Cobble J A, Fernandez J C, Johnson R P, Phys. Rev. Lett. 2001; 87, 155001/1-4

[27] Montgomery D S, Cobble J A, Fernandez J C, Focia R J, Johnson R P, Renard-LeGalloudec R P, Rose H A, Russel D A. Phys. Plasmas 2002; 9, 2311

[28] Nikolic L, Skoric M M, Ishiguro S, Sato T. Phys. Rev. E 2002; 66, 036404

[29] Sircombe N J, Arber T D, Dendy R O. Aspects of Electron Acoustic Wave Physics in Laser Backscatter from Plasmas. Plasma Phys. Controlled Fusion 2006; 48, 1141-1153

[30] Shoucri M. Integration of the Vlasov Equation along Characteristics in One and Two Dimensions. Comp. Phys. Comm. 2003; 154, 65-75

[31] Pohn E, Shoucri M, Kamelander G. Eulerian Vlasov Codes. Comp. Phys. Comm. 2005; 166, 81-93

[32] Bers A, Shkarofsky I P, Shoucri M. Relativistic Landau Damping of Electron Plasma Waves in Stimulated Raman Scattering. Phys. Plasmas 2009; 16, 022104/1-6

[33] Shoucri M. The Sidebands Instability. J. Plasma Phys. 2006; 72, 861-864

[34] Brunner S, Valeo E J. Phys. Rev. Lett., 2004; 93, 145003/1-4

[35] Labaune C, Bandulet H, Depierreux S, Lewis K, Michel P, Michard A, Baldis H A, Hulin S, Pesme D, Hüller S, Tikhonchuk V, Riconda C, Weber S. Laser-Plasma Interaction Experiments in the Context of Inertial Fusion. Plasma Phys. Control. Fusion 2004; 46, B301-B312

[36] Vu H X, DuBois D F, Bezerrides B. Kinetic Inflation of Stimulated Raman Backscatter in Regimes of High Linear Landau Damping. Phys. Plasmas 2002; 9, 1745-1763

[37] Valentini F, O'Neil T M, Dubin D.H.E. Excitation of Nonlinear Electron Acoustic Waves. Phys. Plasmas 2006; 13, 052303/1-7

[38] Kline J L, Montgomery D S, Bezerrides B, Cobble J A, DuBois D F, Johnson R P, Rose H A, Yin L, Vu H X. Observation of a Transition from Fluid to Kinetic Nonlinearities for Langmuir Waves Driven by Stimulated Raman Backscatter. Phys. Rev. Lett. 2005; 94, 175003/1-4

[39] Bénisti D, Gremillet L. Nonlinear Plasma Response to a Slowly-Varying Electrostatic Wave, and Application to Stimulated Raman Scattering. Phys. Plasmas 2007; 14, 042304

[40] Rousseaux C, Baton S D, Bénisti D, Gremillet L, Adam J C, Héron A, Strozzi D J, Amiranoff F. Experimental Evidence of Predominantly Transverse Electron Plasma Waves Driven by Stimulated Raman Scattering of Picosecond Laser Pulses. Phys. Rev. Lett. 2009; 102, 185003/1-4